The Potsdam Soil Moisture Observatory: High-coverage reference observations at kilometer scale

Peter M. Grosse[1,2], Elodie Marret[1], Lena Scheiffele[1], Katya Dimitrova Petrova[1], Till Francke[1], Daniel Altdorff[1,3], Maik Heistermann[1], Merlin Schiel[1], Carsten Neumann[4], Daniel Scheffler[4], Mehdi Saberioon[4], Matthias Kunz[4], Miroslav Zboril[5], Jonas Marach[5], Marcel Reginatto[5], Anna Balenzano[6], Daniel Rasche[7], Christine Stumpp[8], Benjamin Trost[9], and Sascha E. Oswald[1]

[1]Institute of Environmental Science and Geography, University of Potsdam, Karl-Liebknecht-Straße 24–25, 14476 Potsdam, Germany
[2]UFZ - Helmholtz Centre for Environmental Research GmbH, Dep. Monitoring and Exploration Technologies, Permoserstr. 15, 04318 Leipzig, Germany
[3]UFZ - Helmholtz Centre for Environmental Research GmbH, Dep. Computational Hydrosystems, Permoserstr. 15, 04318 Leipzig, Germany
[4]GFZ Helmholtz Centre for Geosciences, Section Remote Sensing and Geoinformatics, Telegrafenberg, 14473 Potsdam, Germany
[5]Physikalisch-Technische Bundesanstalt (PTB), Bundesallee 100, 38116 Braunschweig, Germany
[6]Consiglio Nazionale delle Ricerche (CNR), Area della Ricerca di Bari, Via Amendola 122/D-O, 70126 Bari, Italy
[7]GFZ Helmholtz Centre for Geosciences, Section Hydrology, Telegrafenberg, 14473 Potsdam, Germany
[8]BOKU University, Soil Physics and Rural Water Management, Muthgasse 18, 1190 Vienna, Austria
[9]Leibniz Institute for Agricultural Engineering and Bioeconomy (ATB), Max-Eyth-Allee 100, 14469 Potsdam, Germany

Correspondence: Lena Scheiffele (lena.scheiffele@uni-potsdam.de)
* The first two authors contributed equally to the publication.

Abstract.

Cosmic-ray neutron sensing (CRNS) has gained popularity for estimating soil water content (SWC) due to its innovative capability to measure at an intermediate ~~scale—a~~ scale—a notable advantage over point-scale sensors, which are often sparsely installed and lead to inaccurate absolute values due to small-scale heterogeneity~~result in uncertain absolute values~~. CRNS serves as a crucial link between small and large scales and has been emerging as a reference measurement for ~~remote sensing algorithm validation for its ability to link the small and large scales. Yet~~validating remote sensing algorithms. However, the sparse availability of long-term datasets limits use of this possibility. Within the ~~framework of project~~ DFG-research unit *Cosmic Sense* and the European SoMMet *21GRD08* ~~, multi-scale~~ project, multiscale soil moisture monitoring was implemented to integrate CRNS with complementary in-situ observations. In this paper, we present harmonized soil moisture data from different sensor types, including a CRNS cluster, shallow soil moisture measurements, and soil moisture profile data, creating a ready-to-use dataset as a reference observation for remote sensing products, covering a highly-instrumented agricultural site in the northeast of Germany. The ~~data include~~ newly established Potsdam Soil Moisture Observatory (PosMO) comprises 16 stationary CRNS sensors ~~, with co-located~~ with point-scale SWC sensors ~~(mostly permanent), two groundwater observation wells, meteorological records,~~ installed at the same locations in different depths and data from intensive manual sampling campaigns (covering SWC, bulk density, organic matter, etc.). This dataset ~~distinguishes itself from prior studies by the increased~~

goes beyond other studies by covering a larger area of approx. 1 km^2 ~~while still having~~ ^{2}, while nevertheless achieving a high sensor density and ~~overlapping footprints of CRNS~~ mostly overlapping CRNS footprints allowing for nearly complete coverage. Complementary measurements of soil properties, vegetation, groundwater, meteorology, and remote sensing imagery provide the context required to interpret the observed soil moisture dynamics across spatial and temporal scales. ~~This allows a reasonable degree of geostatistical interpolation to obtain complete coverage.~~ The data are available ~~under the (Grosse et al., 2025) , providing~~ at https://doi.org/10.23728/b2share.bxamy-4zh855 and provide a new reference ~~data set~~ dataset for remote sensing products, hydrological or land-surface models~~and for other products linked~~ , and other applications related to soil water balance.

1 Introduction

The dynamic storage of water in ~~the~~ soil is an important ~~, but spatially and temporally strongly varying part of the water cycle and critical for the exchange fluxes~~ component of the terrestrial water cycle, yet it exhibits pronounced spatial and temporal variability. It regulates water and energy exchange between land surface and atmosphere ~~, ecohydrology, agriculture, forestry~~ and plays a key role in ecohydrological processes, agricultural productivity, forest dynamics and groundwater recharge. ~~Consequently,~~ Due to its critical influence on weather, climate, hydrology, and ecosystem functioning, soil moisture has been ~~identified~~ designated as one of the Essential Climate Variables (Bojinski et al., 2014). ~~Its monitoring is not only related to research from climate science to ecology~~Reliable soil moisture observations are therefore needed not only for climate and ecological research, but also ~~to applied science on~~ for applied purposes including water resources management, ~~flood forecasting, drought monitoring, irrigation management in cropped fields and weather forecasting~~ irrigation planning, and agricultural management, as well as flood and drought forecasting and weather prediction (Vereecken et al., 2008; Brocca et al., 2017; Moragoda et al., 2022; Levi and Bestelmeyer, 2018; Molenaar et al., 2024; Srivastava, 2017; Hövel et al., 2025; Pendergrass et al., 2020; Abioye et al., 2020; Lachenmeier et al., 2024; Szilagyi and Franz, 2020). ~~Main challenges are the observation at different scales, limited direct coverage of~~ Major challenges include the need to observe soil moisture across multiple spatial scales, the limited ability to directly capture root-zone ~~soil moisture and deep storagein soils, and uncertainties and discrepancies between satellite remote sensing~~ and deeper soil water storage, and the spatial and depth mismatches between satellite observations and in-situ measurements (Oswald et al., 2024). Accurate measurements for spatial scales beyond the point scale ~~continue to be challenging~~remain challenging, as small-scale ~~variability caused by~~ variation due to heterogeneity in precipitation, soil properties, vegetation, and other influences question the applicability of point-scale sensors to achieve good spatial and temporal coverage beyond the spot measurement (Peng et al., 2021). Point-scale observations range from campaign-based manual soil sampling to long-term observations using dielectric permittivity-based methods (time-domain reflectometry, frequency-domain reflectometry, capacitance-based sensors) or suction-based methods. These techniques provide observations ~~at~~ with high temporal resolution but due to their small support volume (typically ~~just~~ only a few cubic centimeters) at ~~very specific locations (Robinson et al., 2008)) and the above-mentioned~~ selected locations only (Robinson et al., 2008). Thus, due to the aforementioned heterogeneity of soil ~~water content (SWC)~~moisture, their rep-

resentativeness remains limited. ~~Combined in networksthey offer the possibility to observe representative field-scale soil moisture data (Bogena et al., 2022; Rosenbaum et al., 2012), however, to upscale the point-scale data to an area representative soil moisture is challenging due to the resource-intensive nature of these networks and the conflict with soil management in agricultural settings, where soil moisture observations are of high interest~~When deployed as networks, these sensors enable representative observations of volumetric soil moisture content, in the following called soil water content (SWC) at the field scale (Bogena et al., 2022; Rosenbaum et al., 2012). However, installing and operating sensor networks is resource-intensive and may interfere with agricultural management practices, especially tillage, and thus are limited in areas where soil-moisture observations could be particularly informative.

Over the past decades, satellite-based remote sensing has significantly advanced the ~~measurement~~ assessment of SWC from space. The most notable progress has been achieved using microwave sensors, which offer the distinct advantage of being operable under all weather conditions and during both day and night~~. However, remote sensing estimates of SWC refer to the upper few centimeters of the soil and are acquired at~~ , however with the temporal intervals determined by the satellite's observation schedule. Global-scale SWC measurements with spatial resolutions of approximately 25 × 25 km^2 or coarser ~~, and high temporal frequency (every~~ and a temporal frequency of 2–3 days~~)~~, are currently available e.g. through missions such as the European Space Agency's Soil Moisture and Ocean Salinity (SMOS) mission (Kerr et al., 2001) ~~,~~ or NASA's Soil Moisture Active Passive (SMAP) mission (Entekhabi et al., 2010). Furthermore, the long-term Copernicus program, via the Sentinel-1 (S-1) radar satellites, is fostering the development of operational SWC monitoring at higher spatial resolutions, down to 1 km (Bauer-Marschallinger et al., 2019). The quality assessment of satellite-derived SWC products heavily depends on ground-based measurements (Dorigo et al., 2021). ~~However, a critical challenge remains: the scale mismatch between~~ A persistent challenge in this context is the mismatch not only in spatial scale between the relatively coarse satellite footprints and point-based in-situ observations, but also in depth, as satellite sensors primarily capture near-surface soil moisture while ground measurements often represent deeper layers (Gruber et al., 2020). This mismatch complicates the ~~spatial resolution of ground reference data and that of satellite observations, which poses a significant barrier to the~~ accurate validation ~~of remote sensing products(Gruber et al., 2020)~~and interpretation of remote-sensing products.

Introduced in 2008 (Zreda et al., 2008), Cosmic-Ray Neutron Sensing (CRNS) technology has ~~emerged and meanwhile~~ proven to be a valuable method for intermediate-scale soil moisture measurements, applicable in different land-use and vegetation settings, including forest (Rivera Villarreyes et al., 2011; Baatz et al., 2015). The non-invasive detector retrieves soil moisture time series by detecting the intensity of epithermal neutrons present above ground. This epithermal neutron count rate is inversely correlated to soil moisture, or more precisely, the hydrogen content within its support volume, termed "sensor footprint" in this context, extending vertically about 15 to 60 cm and horizontally about 150 to 200 m radius (Köhli et al., 2015; Schrön et al., 2017). ~~The neutron~~ Neutron counts are typically accumulated over ~~a period of hours, corrections for other~~ several hours, yielding neutron count rates, that are corrected for influencing factors such as air pressure~~applied, and converted to volumetric~~ , and then converted to soil water content using a custom calibration function (Desilets et al., 2010; Zreda et al., 2012). Significant advancements have been made in the past decade in ~~areas such as signal correction (McJannet and Desilets, 2023), interpretation (Köhli et al., 2021; Schrön et al., 2023; Rasche et al., 2021)~~signal correction (e.g. Baatz et al., 2015; Schrön et al., 2018; Mc

, interpretation (e.g. Köhli et al., 2021; Schrön et al., 2023; Rasche et al., 2021), sensor calibration/uncertainty reduction ~~(Schrön et al., 201~~
(e.g. Schrön et al., 2017), and data processing ~~(?)~~(e.g. Power et al., 2021b, 2025). As a result, ~~Cosmic-Ray Neutron Sensor~~ CRNS technology is increasingly ~~utilized~~ tested for diverse applications, besides soil ~~moisture content measurements also for biomass estimation (Jakobi et al., 2018; Brogi et al., 2022)~~water content measurements it could alternatively also give an estimate of biomass or interception (Baroni and Oswald, 2015; Jakobi et al., 2018; Brogi et al., 2025) or is used for irrigation assessment (Brogi et al., 2022), and observations of snow water equivalent ~~(Schattan et al., 2017). However, its major advantage - providing a~~ (Schattan et al., 2017; Bogena et al., 2020). Overall, the major advantage of CRNS is its ability to provide a time-resolved, large-scale~~and integrative soil moisture measurement within the critical root zone - remains underutilized so far~~, and integrative measurement of the so-called root-zone soil moisture (RZSM), representing soil water storage in the upper decimeters of the soil profile. This zone typically contains the highest root densities for many many vegetation types and thus constitutes a key component of soil water storage and the critical zone. Consequently, CRNS captures a substantially larger fraction plant-available soil water than the so-called surface soil moisture (SSM) retrieved commonly by satellite remote sensing. Nevertheless, it has remained underutilized in its first decade, though for some years now there are studies actually employing CRNS data in hydrological modeling, deriving water fluxes or snowmelt using the CRNS data, beyond merely comparing their results to it (see e.g. Shuttleworth et al. (2013); Barbosa et al. (2021); Patil et al. (2021); Scheiffele et al. (2025); Arnault et
. This can largely be attributed to the ~~relative~~ initial sparseness of sufficiently-long records, ~~and~~ the required expertise in their conversion to soil ~~moisture. Nevertheless, despite all the corrections and advancements, the basic ability of the sensor was there from the start - the very large advantage of measuring non-invasively, averaging out the effects of small-scale heterogeneities in its signal~~water content and technical questions of directly using CRNS-derived root-zone soil moisture in modeling.

The non-invasive and low-maintenance nature of CRNS technology, ~~combined~~ together with its ability to ~~record data over long periods, made it a promising~~ to provide long-term continuous observations, makes it a highly suitable tool for remote sensing assessments (Babaeian et al., 2018; Mengen et al., 2023; Beale et al., 2021). ~~While~~ Although various CRNS-datasets have been published (e.g. Bogena et al., 2022; Cooper et al., 2021; Dorigo et al., 2021), they are mostly composed of solitary, i.e. spatially detached, stations. ~~Although single-footprint sizes represent a major step~~ While the footprint of an individual CRNS already marks substantial progress toward matching the spatial resolution of remote sensing products (Meyer et al., 2022) , they still fall short of the ~~spatial resolution required by some~~ pixel size used by many applications. Combining multiple ~~CRNS-sensors~~ CRNS sensors in close vicinity ~~remedies this issue~~helps addressing these spatial limitations. By establishing dense CRNS station networks, so called CRNS clusters, recent studies have begun to ~~address the lack of comprehensive datasets: these CRNS sensors are operated with~~ fill the gap of comprehensive spatial datasets: overlapping or adjacent ~~footprints providing a robust option for~~ CRNS footprints provide a robust means of capturing the spatial and temporal ~~distribution~~ variation of soil moisture in the covered area. To date, three such data sets have been published. At the pre-alpine agro-sylvo-pastoral headwater catchment site in Fendt, 24 CRNS sensors were ~~installed over a~~ deployed across 1 km^2 ~~area for a short period of two months~~ for a two-month period (Fersch et al., 2020). In 2020, ~~at the Wüstebach catchment in the Eifel Mountains,~~ 15 detectors were operated ~~over~~ for three months in the 0.4 km^2 ~~of forested land temporary for three months (Heistermann et al., 2022). More~~ forested Wüstebach catchment in the Eifel Mountains (Heistermann et al., 2022). Most re-

cently, Heistermann et al. (2023) ~~reported the data from~~ presented three years of observations from a high-density cluster of 15 CRNS ~~sensors over a~~ stations installed over 0.1 km^2 ~~lowland agricultural site at the~~ of lowland agricultural land at the Marquardt site of the Leibniz-Institut für Agrartechnik und Bioökonomie (ATB)~~Marquardt~~. The latter cluster was the only one ~~designed for a longer-term operation , i.e. more than a year, and specifically has aimed for being able to account for local heterogeneities by its unusual high-density of CRNS detectors~~explicitly aiming for long-term operation (i.e. beyond one year) and was intentionally configured at unusually high density to exploit the strongly overlapping CRNS footprints, together with inversion techniques, to resolve sub-footprint heterogeneity.

The ~~current study combines the scale of coverage of the temporary Fendt site investigation with the continuity of observation of the ATB Marquardt site . It was implemented on remaining parts of the former CRNS cluster at the latter site and extended to an area that is larger by an order of magnitude. By that it does not only cover now the complete ATB site, but goes beyond and even includes areas within two communes being part of the City of Potsdam. That is what we will refer to here as the *Potsdam Soil Moisture Observatory* (PoSMO) .~~

~~The new cluster, installed on a well-controlled agricultural field with on-site weather records, was designed to be able to provide a reference soil moisture dataset~~ *Potsdam Soil Moisture Observatory* (PoSMO) replaces the former high-density cluster at the ATB site and was established to provide spatially representative reference data for validating high-resolution satellite soil moisture products and for capturing hydrological extremes. Its design was guided by the following objectives (i) to exploit the footprint sizes of the CRNS more completely than before; (ii) to cover an area of about 1 km^2, with a denser coverage at the core and a looser coverage at the outer parts; (iii) to keep some of the former CRNS stations (position and device) to provide long-term time series continuing former observations, as valuable e.g. for satellite remote sensing ~~. Compared to Heistermann et al. (2022), it extends instrumentation to~~ comparison; and (iv) to enable a closer link to surface soil moisture remote sensing observations by adding shallow point scale sensors.

PoSMO integrates 16 distributed CRNS sensors with complementary point-scale soil moisture measurements from shallow depths consistent with remote-sensing penetration depths to profiles down to 1 ~~m~~, enabling both horizontal and vertical characterization of soil water dynamics. Operational since mid-December 2023, PoSMO covers approximately 1-3 km^2 ~~to match the resolution of highly-resolved satellite remote sensing products, maintains a continuous time series since 2019 (seven sensorsfrom the previous cluster) to better capture hydrological extremes, and adds complementary datasets (hyperspectral and Lidar data, stable isotopes, electrical resisitvity tompgraphy, etc.) to~~ ^{2} of predominantly agricultural land and provides continuous soil moisture observations under a wide range of hydrological conditions, including droughts, heavy rainfall, irrigation events, and snow cover.

Complementary data sets enhance soil moisture reconstruction at the km^2 scale~~. Besides the soil moisturefrom CRNS, point-scale soil moisture profiles from 10 cm down to 1 m were measured in combination~~ , including several intensive campaigns for CRNS calibration (soil moisture, bulk density, texture and soil hydrogen pools), hyperspectral and Lidar data, stable water isotopes, electrical resistivity tomography, and others. SWC monitoring at PoSMO is intended to be continued further, to finally be able to provide a three-years data set (as a future update to the first data set presented in the current paper).

In the following we will introduce the field site with the CRNS ~~sensors and these were supplemented by even shallower point-scale soil moisture measurements, aligning with the penetration depth of remote sensing products and reflecting the standard commonly used for their validation~~installation and supporting instrumentation, describe in detail the observations, data processing and calibration workflow, and finally present exemplary results illustrating key dynamics in the dataset and highlight future applications of PoSMO as a long-term reference site for remote sensing and hydrological research.

2 Study Area and Instrumentation

2.1 ~~General description~~

~~In 2019,~~

The *Potsdam Soil Moisture Observatory* (PoSMO) has been established by the University of Potsdam ~~began operating a dense CRNS cluster at~~ at and around an agricultural research site located in the ~~Potsdam-Marquardt site as part of the Cosmic Sense project, named the "Marquardt cluster". This site, located in northeastern Germany in the~~ northwest of Potsdam ~~, has since then been expanded as a key long-term soil moisture monitoring observatory. The major part of the PoSMO is now distributed over the whole research site~~ in northeastern Germany, which is operated by the ~~Leibniz Institute for Agricultural Engineering and Bioeconomy (ATB), but some stations cover areas outside the ATB site and a few are located completely outside of it. Recent investigations have been part of~~ ATB. In its central part the DFG research unit *Cosmic Sense* ~~and~~ had operated a dense CRNS cluster since end of 2019, referred to as the "Marquardt cluster". This cluster was originally designed to exploit strongly overlapping CRNS footprints for assessing sub-footprint soil moisture heterogeneity. Within the second phase of *Cosmic Sense* and for the interdisciplinary EURAMET (European Association of National Metrology Institutes) project *21GRD08 SoMMet*~~running until end of 2025 and September 2025, respectively~~, a new cluster setup was envisioned, now as a key long-term soil moisture monitoring observatory at km^2 scale. The main aim has been the observation and harmonization of soil ~~moisture~~ water content across multiple spatial and temporal scales. ~~The automated observations are scheduled to be continued beyond the projects' time frames, so that the published dataset could be updated in the future.~~ To achieve that, the newly-created PoSMO was implemented by repositioning and refurbishing some of the existing CRNS stations but also by deploying a number of additional CRNS stations, a station setup consisting of CRNS senor, dielectric profile and single-depth soil water content sensors. By that the former cluster was not only extended by nearly an order of magnitude, but now includes cropped fields larger in size than before, also outside the fenced ATB site. To further increase the spatial coverage of PoSMO, a suitable location with similar land use and soil type was selected approximately 2 km east of the ATB (Fig. 1).

~~The PoSMO consists of an inner~~

Figure 1. Locations of CRNS stations at the Potsdam Soil Moisture Observatory (PoSMO). Numbers refer to the station IDs, a station consisting of a CRNS device and point-scale shallow and profile soil moisture sensors installed in close proximity. The purple area indicates the extent of predominantly agricultural land with broadly similar land use and soil types, representing land-use unit that PoSMO aims to characterize and provide reference data at landscape scale and that is consistent with the spatial aggregation of satellite soil-moisture products (forest and settlement areas excluded). Background image from Google Earth (retrieved in September 2023 (Gorelick et al., 2017), Maxar Technologies).

As a result, the denser cluster in the western part of PoSMO provides an actual soil moisture measurement covering the complete area of the ATB site including its immediate surroundings (approximately 0.7 km^2) under mixed agricultural land use. This is achieved through overlapping or adjoining horizontal CRNS footprints of multiple CRNS stations distributed across the fenced ATB site. The coverage is expanded by one CRNS station directly east of the ATB site and especially the more isolated easternmost CRNS station, both reflecting a more typical remote sensing validation setup, with one station representing a rather homogeneous land use in its surrounding (Schmidt et al., 2024). Altogether PoSMO could be taken to represent an area of about ~~0.7~~ 3.4 km^2 ~~area~~ of predominantly cropped fields and meadows, with some other agricultural land use and loose urban settlings (Fig. 1). The current setup thus combines the scale of coverage of the first temporary CRNS cluster at the Fendt site Fersch et al. (2020) with the continuity of observation of the ATB Marquardt site Heistermann et al. (2023).

The ATB site, as the most densely instrumented western area of PoSMO, is located at 40 m a.s.l. ~~, including~~ on a gentle hillslope sloping towards the lake in the west and characterized by diverse experimental agricultural plots (Fig. 2). Crops grown include cereals, maize, alfalfa, sunflower, ~~rape seed, meadows, diverse types~~ and rape seed; the site also features meadows, a variety of orchards (cherry, apple, ~~maroni) and young poplars—under rain-fed management~~chestnut) and a poplar short-rotation plantation. With exception of a few irrigated orchards and ~~local irrigation measures~~ occasional local irrigation (on potatoes,

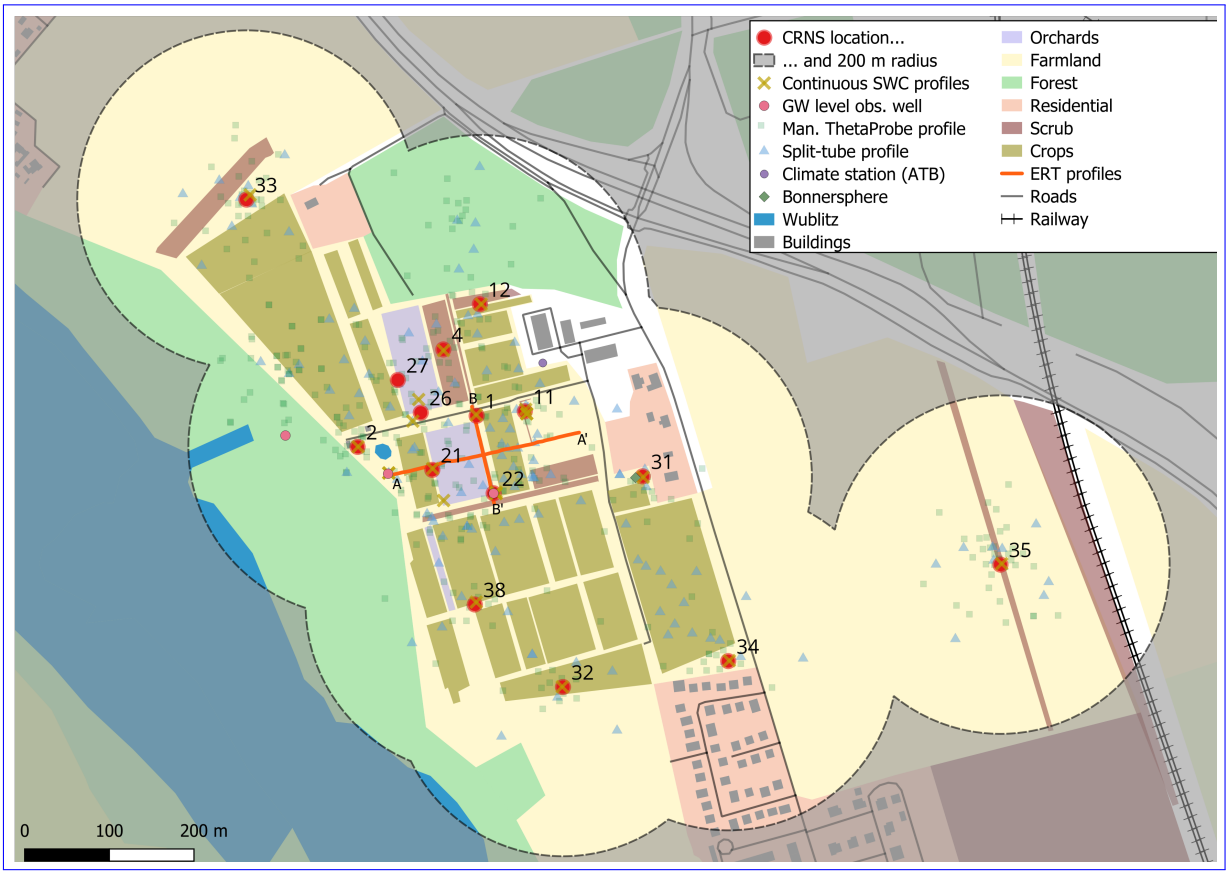

Figure 2. Overview of the main part of PoSMO, showing continuously operating CRNS stations with the numbers showing their ID (a station includes a CRNS detector, point-scale shallow and profile soil moisture sensors), as well as groundwater monitoring wells and climate station. The approximate horizontal footprint of the CRNS detectors, based on a 150 m radius, is given as highlighted area, with the envelope of the area covered indicated as dashed line. Additionally the map shows the two ERT transects, hyperspectral camera position, Bonner sphere spectrometer location and calibration sampling points (Manual ThetaProbe profile and Split-tube profile). Background layers illustrate land use such as farmland, buildings, lake and forested areas that are based on OpenStreetMap (OSM) with few amendments.

maize and spring wheat), the site is ~~under rain-fed management. It features 20 agricultural field plots and~~ mainly rainfed. The observatory is situated on predominantly periglacial ~~sandy soils (~~deposits with sandy to loamy topsoil (0 to 50 cm depth) and soil texture ranging from 68–91% ~~), with silt content ranging from~~ sand, 8–27% ~~and clay from~~ silt, 0.6–4.4% ~~. Organic matter content ranges from~~ clay, and organic matter contents between 0.4–17.3% (by mass). The climate is temperate, with an ~~average~~ mean annual precipitation of 584 mm (1981-2010) and an ~~average~~ mean annual temperature of 9.3°C (Cfb by Köppen-Geiger). The groundwater table lies between 1.5 and 10 m beneath the surface, and two observation wells ~~installed in 2019 continue to provide data. Two weather stations, that is one on-site and one located~~ were installed in 2019. Comprehensive meteorological observations are provided by an on-site weather station, a second station 5 km away (both operated by ATB), and a third station 12 km away operated by the German Meteorological ~~service~~ Service (DWD) ~~, ensure comprehensive meteorological observations~~(details see section 4).

The site is representative of typical lowland agricultural landscapes in northern Central Europe, situated within a climatic transition zone between maritime and continental influences. Moderate seasonal contrasts allow the site to capture a broad range of hydro-meteorological conditions relevant to temperate agro-ecosystems. As such, the site serves as a valuable model ~~enviroment~~ environment for investigating soil moisture dynamics across diverse hydro-climatological conditions, including dry periods, snow events, and variable precipitation patterns. ~~Its setting enhances the transferability of findings to similar agricultural contexts across the region.~~

~~Locations of cluster stations (CRNS, shallow SWC, SWC profile) at the Potsdam soil moisture observatory. The total area of mixed agricultural land use that the observatory represents could be taken as the purple area (size of 3.4 km^2, similar land use, soil type and aligning with the spatial extent of remote sensing products, excluding forest and settlement areas). The background image is taken from Google Earth: Marquardt, retrieved in September 2023 (Gorelick et al., 2017) , Maxar Technologies.~~

2.1 ~~Highlights of PoSMO~~

~~The Potsdam soil moisture observatory (PoSMO) stands out for several reasons: With 15 CRNS stations distributed over an area of approximately 0.7 km^2, it covers an area seven times as large than the previous CRNS cluster. The CRNS locations were placed in order to monitor both vertical and horizontal soil moisture variability, with one additional CRNS location placed 2 km east to extend the spatial coverage even further. Similar land use and soil types render the sensor highly representative of the broader surroundings at the resolution of remote sensing products (excluding forested area and settlements). Altogether PoSMO could be taken to represent an area of about 3 km^2 of predominantly cropped fields and meadows, with some other agricultural land use and loose urban settlings (Fig. 1).~~

~~PoSMO has been operational in its present form since mid December 2023, allowing observations under varied conditions, including snow events (e.g., snow covered the site for eight days in February~~ Although the two research projects *Cosmic Sense* and *SoMMet* that initiated and supported the establishment and operation of the observatory have finished end of 2025~~),~~ ~~drought, irrigation, and heavy rainfall. Monitoring is intended~~ , automated measurements are scheduled to be continued ~~, to finally be able to provide a three-years data set (as a future update to the first data set presented in the current paper).~~

~~The test site incorporates diverse land uses and features—including croplands, roads, buildings, though dominated by agricultural area, providing an ideal setup for assessing soil moisture dynamics under contrasting conditions.~~

~~Extensive instrumentation complements the CRNS data. Two SMT100 TDT sensors (Truebner) were installed in December 2023 at each of~~ by University of Potsdam at least until end of 2026, allowing for future updates of the ~~16 cluster locations at 5 and 15 cm depth (totalling to 32 sensors), adding to the 20 soil moisture profile measurements (including PR2/4, PR2/6, ThetaProbes ML2x, TDR) that cover depths from 10 down to 100 or 200 cm. Faulty sensors were regularly replaced to maximize data continuity.~~ published dataset.

~~Soil moisture measurements include a rich dataset of manual and automated readings. In 2023, six calibration campaigns were conducted (in May, July, October and November), covering 145 locations. Manual FDR measurements were collected at six depths, with 33 locations including full soil sampling. In 2024, in four additional campaigns (in April, August and October), 138 new FDR samples and 32 soil bulk density sampling points were taken.~~

~~Soil bulk density is a key parameter for deriving volumetric soil moisture from CRNS observations, just as it is essential for retrieving soil moisture from saturation- or index-based remote sensing products, for hydrological applications, and for simulating CRNS signals in the field. Bulk density values were interpolated from 136 locations at PoSMO including campaigns since 2019 (cf. Fig. 7).~~

~~Larger snow cover events have also been monitored. Thus, a dedicated snow campaign on the 17 February 2025 included 240 snow height measurements, 10 snow bulk density samples, UAV imaging, and wildlife camera deployment to monitor melting.~~

~~To unravel the relationship between soil moisture dynamics and downward soil water fluxes, bulk soil water samples were analysed for stable water isotopes on three occasions and interpretation was aided by dedicated measurements of saturated hydraulic conductivity in the root zone. Measurements were distributed to capture spatial heterogeneity, stemming from the mixed land use covers.~~

~~Overview of the Potsdam soil moisture observatory central area, showing continuously operating stations (CRNS, SWC profiles, groundwater monitoring, tensiometers, and climate stations), the two ERT transects, hyperspectral camera position, Bonner sphere spectrometer location and calibration sampling points. Background layers illustrate land use such as farmland, buildings, and forested areas etc. are based on OpenStreetMap (OSM) with few amendments.~~

3 Observations and ~~data~~methods

The following subsections provide an overview of the instruments and related observations that comprise the dataset. Table 1 summarizes the various sub-datasets collected~~from 2023 to 2025, during which period also five drought events (all CRNS sensors providing soil moisture < 15 %) and three extreme precipitation events were observed (daily precipitation over 20 mm). The core components of the dataset include the distributed CRNS stations, vertical soil water content profiles and shallow soil water content time series, remote sensing data, all of which are described in detail in Section 3.1.1 and listed in Table 1.~~ .

Table 1. Overview of section 3: brief summary of each data subset, main observed variables~~and~~ , units, and temporal coverage. Specific details ~~can be found~~ are given in the corresponding subsections and in the ~~json~~ accompanying JSON files, which ~~documents~~ document each ~~data~~ subset ~~in~~ within the repository. ~~The text~~ Folder names (shown in bold~~indicates~~) follow the ~~name~~ section numbering of the ~~folder~~ manuscript, with ~~these data sets~~ each numbered folder in the ~~repository, which will be preceded by~~ dataset containing the ~~number on~~ data described in the ~~left~~respective section.

Sect.	Data subset	Main observation variables (units)	Temporal coverage
3.1.1	**Stationary CRNS data**, 16 ~~permanent **stationary CRNS detectorsrecorded**~~ detectors, hourly time series of epithermal neutron counts~~along with meteorological variables~~, meteorological variables, and CRNS-derived soil moisture	~~neutron count rate (eph~~Neutron counts (-), air pressure (hPa) and temperature (°C), relative humidity (%), SWC (m^3 m^{-3})	Dec ~~2023-Jul~~2023-Oct 2025
~~3.5~~ 3.2	~~One **muondetector to represent temporal variability of incoming fast neutrons, as potential correction for CRNS data muon count rate (eph**~~**Campaign-based manual soil sampling** for CRNS calibration, upper 30 cm of the soil (gravimetric samples and dielectric measurements)	~~Feb 2023-Jul 2025**?? Neutron spectrum** recorded as daily values by a group of outdoor Bonner spheres, as potential correction for CRNS data and detector response histogram (eph)Jun~~ SWC (m^3 m^{-3}), permittivity (-~~Jul 2025~~), bulk density (g cm^{-3}), organic matter content (g g^{-1}), soil texture (mass %)	May 2023-Oct 2024
3.3	~~**SWC**~~ **Soil moisture profiles**~~**time series**~~ , hourly time series from dielectric profile sensors at 20 locations (~~dielectric measurements~~10 to 100 cm)	Permittivity (-), SWC (m^3~~/m^3~~ m^{-3})	Dec ~~2023-Jul~~2023-Oct 2025
3.4	**Shallow ~~SWC~~~~time series~~ soil moisture** and temperature, hourly time series from dielectric point sensors at 16 locations (~~via TDT~~5 and 15 cm)	Permittivity (-), SWC (m^3~~/m^3~~) ~~, Soil~~ ^{3} m^{-3}) , soil temperature (°C)	Dec ~~2023-Jul~~2023-Oct 2025
~~3.2~~ 3.5	~~Multiple campaigns with **manual soil samplingof the upper 30 cm of the soil (split-tubes, ThetaProbes, lab analysis)**~~ **Muon data**, hourly time series from one scintillator-based CRNS detector	~~Permittivity, SWC (m^3/m^3) , bulk density (g/cm^3) , SOM (g/g), texture~~ Muon count rate (cph)	~~May 2023-Oct~~Feb 2023-Jul ~~2024~~20
3.6	**Neutron spectrum** recorded as daily values by a group of outdoor Bonner spheres	Neutron energy histogram (cph)	Jun-Jul 2025
3.7	**Hyperspectral reflectance** time series ~~on-ground~~ of soil surface, terrestrial sensor	Reflectance (-)	Oct 2022-May 2024
3.8	**Hyperspectral airborne imagery** at one date	Reflectance (-)	Sep 2024
3.9	**Airborne Lidar imagery** at one date	Digital Surface and Terrain Model (m) ~~,~~	Sep 2024
3.10	**Landuse**, especially crop cycles	~~sowing and~~harvest ~~Sowing and~~ harvest dates	Apr 2021-Jul 2025
3.11	**Snow** depth monitoring and ~~some~~ snow sampling (various techniques), areal imagery mosaics from an UAS overflight	Snow water equivalent (SWE) (mm), snow depth (cm)~~and~~ , density (g~~/cm~~ cm^{-3}); RGB mosaic	Feb 2025
3.12	**Groundwater level** and lake level time series (hourly)	GW level (m.a.s.l.)~~and~~ , distance to surface	Dec 2023-Jun 2025

3.1 ~~Soil moisture from stationary~~ Stationary CRNS data

3.1.1 CRNS sensor installation

From December 2023 to ~~April~~ October 2025, we collected epithermal neutron count data from 16 stationary Cosmic-Ray Neutron Sensors (CRNS) ~~with overlapping footprints~~ at the soil moisture observatory established in Potsdam ~~. The locations~~ (PoSMO). The positions of the CRNS sensors are depicted in Fig. 1 and 2. The placement of the sensors was ~~informed by~~ selected based on several key considerations: (i) to ensure a substantial overlap of the footprints, (ii) to capture the site's variability along the hillslope gradient, (iii) to position some sensors near the groundwater ~~well, and~~ wells, (iv) to avoid interfering with agricultural management activities, which necessitated ~~not to directly place sensor on cropped~~to not directly place sensors on cultivated areas, and (v) to extend the spatial coverage for direct comparison with remote sensing products, while placing the sensors to largely homogeneous surroundings.

The detailed specifications of the ~~sensor cluster~~ sensors installed at the observatory are provided in Table 2, including the manufacturer, sensor type, and detector sensitivity (for further details, see Heistermann et al. (2023)). A total of 16 sensors from various manufacturers were included in the study: five devices from Hydroinnova LLC (Albuquerque, USA), four from Quaesta Instruments LLC (Tucson, USA), four from StyX Neutronica GmbH (Mannheim, Germany), one Canberra (now Mirion Technologies, USA), one from Finapp S.r.l. (San Pietro in Cariano, Italy), and one from Lab-C LLC (Sheridan, USA), which is now associated with Quaesta Instruments. The sensitivity of each device was determined through parallel measurements with a reference CRNS sensor (calibrator) over a ~~test period~~ period of at least 24 hours, allowing for a comparison of the neutron count rates observed by different instruments. The detector sensitivities (Table 2) would allow to process the neutron counts of all sensors with a universal calibration parameter to derive CRNS soil moisture (Heistermann et al., 2024). As detailed in Table ~~2~~2, the majority of the ~~detectors~~ devices employ gases with high neutron cross-sections to detect neutrons, including ^{3}He gas (CRS-1000, CRS-2000) and $^{10}BF_3$ enriched gas (CRS-1000B, CRS-2000-B, B-E1-4). The 'HydroSense Dual' detector is based on a multiwire proportional chamber with solid ^{6}Li (Fersch et al., 2020; Patrignani et al., 2021), while the StX-140-5-15 sensors utilize ^{10}B-lined converters. Finally, the FINAPP5 ~~instrumental detection of neutrons~~ relies on a multi-layer zinc sulfide and ^{100}Ag doped scintillator with ^{6}Li fluoride powder (Gianessi et al., 2024). All of the devices described above are ~~epithermal neutron detectors~~ detectors for epithermal neutrons. Most ~~sensors record also~~ CRNS devices also record temperature, relative humidity, and barometric pressure using ~~an external sensor~~external sensors. These data were used to correct the raw neutron count rates. For sensors without ~~own~~ an external sensor, data from the reference station at location ~~ID~~ #11 were used for corrections. Besides the neutron count time series we also provide processed CRNS soil water content.

~~To exemplify the use of the CRNS observations we have processed the CRNS data to obtain a soil moisture product (Figure 4, see also section 3.1.2), which is also included in the data set. Soil moisture estimates derived from CRNS data are susceptible to various sources of uncertainty, including the influence of other hydrogen pools, which are not explicitly accounted for in this SWC series presented in this paper, but implicitly addressed by the local calibration procedure.~~

~~Figure 4 presents a comprehensive overview of the time series data from December 2023 to 2025. This heat map reveals five major drought events (occurring in summer 2024 and summer 2025) and two notable snow fall events in February 2025.~~

Table 2. Properties of CRNS sensors used ~~in~~ at the ~~Potsdam cluster~~ PoSMO (including manufacturer, model, and detector ~~mechanism~~principle). Also provided is the ratio of the sensor's raw counts of epithermal neutrons to the counts of a calibrator sensor (consistent with Heistermann et al. (2023)), referred to as *sensitivity*. This is a device specific property, which is independent of the site. It can be used to infer a local calibration parameter value (cf. Heistermann et al., 2024)). Some CRNS devices have been refurbished and are technically different to the formerly used device, and thus the sensitivity value had to be updated and is different to the former one. CRNS ~~devices~~ stations that have been continued at their former ~~location~~ position with identical set-up are printed with bold ID. Finapp s.r.l. has changed its CRNS model names; Finapp 3 (F3) refers now to Finapp SWC, Finapp 5 (F5) to Finapp SWC plus, and Finapp 6 (F6) to Finapp SWC Premium. Some Lab-C CRNS devices are currently only ~~provided~~ sold via Quaesta Instruments, and then the manufacturer listed is Quaesta Instruments.

ID	Manufacturer	CRNS type	Detection mech.	Sensitivity	~~remark~~remarks
1	Hydroinnova	CRS 2000-B	$^{10}BF_3$ gas	1.191	
2	Canberra	self-assembled	^{3}He gas	0.668*	refurbished; ~~set-up with horizontal tube position~~ horizontal t
4	Lab-C	HydroSense dual	^{6}Li foil	4.537	
11	Quaesta Instr.	dual BF3-C-4	$^{10}BF_3$ gas	4.871	
12	StyX Neutronica	StX-140-5-15	^{10}B-lined	1.127	refurbished
21	Hydroinnova	CRS 2000-B	$^{10}BF_3$ gas	1.149	
22	Hydroinnova	CRS 2000-B	$^{10}BF_3$ gas	1.163	
26	Quaesta Instr.	B-E1-4	$^{10}BF_3$ gas	2.487	single tube of a dual system
27	Quaesta Instr.	B-E1-4	$^{10}BF_3$ gas	2.468	single tube of a dual system
31	StyX Neutronica	StX-140-5-15	^{10}B-lined	2.773	
32	Finapp s.r.l.	Finapp-SWC Plus	^{6}Li-doted scinti.	1.400	muon sensor included
33	Quaesta Instr.	BF3-A-3, dual	$^{10}BF_3$ gas	1.490	
34	Hydroinnova	CRS 1000	^{3}He gas	0.448	
35	Hydroinnova	CRS 1000	^{3}He gas	0.689	
38	StyX Neutronica	StX-140-5-15	^{10}B-lined	2.425*	
39	StyX Neutronica	similar to SP2	^{10}B-lined	~~2.236~~ 2.425	refurbished
11val	Finapp s.r.l.	Finapp-SWC Premium	^{6}Li-doted scinti.	0.873	not part of the ~~cluster~~PoSMO, as testing option

*type-generic sensitivity factor

~~The temporal dynamics of the 16 locations exhibit consistent patterns over time . To facilitate a straightforward analysis, the sensors have been grouped according to their geographical location, ranging from the west to the east. It should be noted that, if the effect of snow coverage on the CRNS measurements is evident, this was not a focus on this dataset. For the snow episode documented during winter 2024/2025, the snow coverage, the height, and density measurements are independently detailed in this dataset (section 3.11). The precipitation data from the DWD weather station (see section 4) demonstrate the CRNS response to rainfall events.~~

~~Figure 6 shows two examples of the spatial distribution of root-zone soil moisture as inferred from the CRNS~~

3.1.2 CRNS-based soil water content estimation

For the data ~~on 8 September 2024~~ processing of CRNS neutron count time series, the Python tools Corny (Schrön, 2025) and Neptoon (Power et al., 2025) were used. Both tools provide algorithms to filter raw counts for outliers, aggregate them to the desired time interval, correct for atmospheric influences, smooth the time series, and ~~24 November 2024. Spatial interpolation on a 2 m resolution grid takes into account CRNS horizontal sensitivity combined with inverse distance weighting. Among the various sensors, a notable consistency in response patterns can be observed for both wet and dry periods.~~ calibrate the CRNS with independently derived soil moisture data (section 3.2), which is required to convert neutron counts to soil moisture. The data processing involves several subjective choices. To ensure transparency and reproducibility, we provide the full configuration files for Corny and Neptoon in the data repository. This will allow users to understand, reproduce, or adapt the data processing details.

~~(a) Daily precipitation; (b) Root-zone soil moisture time series derived from CRNS measurements, arranged from west to east according to sensor locations. The arrows above the soil moisture time series indicate periods of snow fall that may influence soil moisture dynamics.~~

3.2 ~~Additional muon observation~~

~~Neutron monitors, such as the the one at Jungfraujoch (JUNG) in Switzerland, are conventionally used to correct locally measured epithermal neutron counts for variations in incoming neutrons. Recent studies suggest that local measurements of muon counts could enhance methods for correcting CRNS data to account for incoming~~ The first step in the processing for the CRNS soil moisture products provided in this data set is the filtering of neutron count time series for outliers, which are identified using a standard deviation–based threshold. Count rates are influenced by atmospheric factors; therefore, we applied the following corrections: the effects of barometric pressure were corrected following Zreda et al. (2012); effects of incoming cosmic-ray neutron flux were corrected using the station Jungfraujoch JUNG (Switzerland), following either the approach from Zreda et al. (2012) or Hawdon et al. (2014); effects of atmospheric vapour content were corrected using the method described in Rosolem et al. (2013) or inherently accounted for, depending on the conversion function to soil moisture (calibration function). CRNS time series were calibrated using the revised standard transfer function from Desilets et al. (2010) and the universal transfer function (UTS) function according to Köhli et al. (2021). For calibration, neutron ~~variability (Stevanato et al., 202 . To provide this capability and explore this option, one CRNS sensor operated in the Potsdam cluster (#32)included sensors for detecting muons (Gianessi et al., 2024), and these data are available from January 2023 to May 2025; see also Table 2.~~

~~Root-zone soil moisture distribution for a relatively moist period of the time series in July 2025(left) and for a late summer day of a drier period in September 2024 (right). Root-zone soil moisture distribution based on the daily soil moisture product derived from CRNS stations within the central area of the Observatory (section 3.1.1). Dashed circles outline the 150 m footprint of the sensors. Map background information see Figure 2~~

3.2 ~~Bonner sphere measurements of full neutron energy spectrum~~

An extended range Bonner sphere spectrometer (ERBSS) consists of a set of moderating spheres of different diameters and a thermal neutron detector that is placed at the center of each sphere. A typical set has standard spheres made of polyethylene plus a few modified spheres with metal shells embedded in counts are related to independently determined reference soil moisture, typically derived from in-situ soil sampling campaigns (see section 3.2). This procedure allows the determination of the polyethylene spheres. Each sphere plus thermal neutron detector combination has a different energy response to neutrons. For the standard spheres, the peak of the response function shifts to higher neutron energies as the size of the moderator is increased. For the modified spheres, the response increases dramatically for neutron energies above ~50 MeV. In addition, it is usual practice to measure also with the thermal neutron detector without a moderating sphere (i.e., the bare detector). Any combination of sphere and thermal neutron detector is usually called a "sphere" and this terminology has also been extended to the bare detector.

The Physikalisch-Technische Bundesanstalt (PTB) has been operating its ERBBS system, known as NEMUS Wiegel and Alevra (2002) , for about two decades. Recently, the PTB developed an SI-traceable copy of the NEMUS system specifically for automated neutron spectrometry measurements under outdoor conditions . The system NEMUS-UMW (from the German word *Umwelt* - environment) consists of a new subset of NEMUS spheres: 6 polyethylene ones with diameters of 3, 4, 5, 6, 8 and 10 inches, a bare thermal neutron detector and four modified spheres with lead and copper shells. The central thermal neutron detectors are spherical ^{3}He-filled proportional counters of the type SP9, manufactured by Centronic Ltd. The specific SP9 counters used in the NEMUS-UMW system were selected for low-level neutron measurements due to their low intrinsic background. The intrinsic (instrumental) background of each SP9 counter was systematically tested and quantified in the "neutron-free" environment of the PTB underground laboratory UDO II. The electronics for neutron signal processing and telemetry of the NEMUS-UMW system are comprised of components that correspond to the state of the art in the CRNS community. Using unfolding procedures Reginatto (2010), one can determine the neutron spectrum from the measured data and the spectrometer response functions. The NEMUS response functions were characterized and validated in the PTB's neutron reference fields, site specific calibration parameter N_0 and the NEMUS system serves as a secondary metrological transfer standard for neutron fluence rate measurements. This means that the resulting unfolded neutron spectrum is determined in absolute terms, in units of neutron fluence $\Phi(E)$ in neutrons cm^{-2}. N_D for the two approaches, respectively. While the standard transfer function is most widely used, the newer UTS does specifically accounts for the influence of air humidity on neutron transport and provides more accurate soil moisture estimates especially for dry soil conditions (Rasche et al., 2024). Besides soil moisture, calibration requires information on soil bulk density and hydrogen stored within the subsoil of the sensor footprint. For this purpose, the vertically-generalized profiles of soil moisture, bulk density, lattice water and organic matter were interpolated onto a 1-m-grid and weighted following Schrön et al. (2017). The weighting includes the estimation of the effective sensing depth (D86), also called integration depth, and the horizontal footprint (R86), also called support area; for sampling details see section 3.2. Resulting CRNS soil moisture time series are provided at hourly resolution. Because neutron count time series exhibit high statistical noise, either corrected count rates (prior to conversion) or the resulting soil moisture products must be smoothed. A moving average with a window length of 12-14 hours is commonly applied, although alternative smoothing approaches have been proposed (Franz et al., 2020). CRNS-derived SWC time series are are presented and discussed in section 5.1.

~~Since 18 June 2025,~~

3.2 Campaign-based soil measurements for CRNS calibration

To facilitate the calibration of the ~~NEMUS-UMW system has been operated at the Potsdam site, at a location with permanent power supply as well as close to one CRNS station (#31)~~ CRNS sensors, extensive field campaigns were conducted at 283 new profile locations, complemented by data from two previous campaigns in 2019 and 2022 (Heistermann et al., 2023). This dataset encompasses a total of 38 campaigns within the CRNS footprints, with both dielectric and soil core measurements taken down to a depth of 35 cm. In total, dielectric profiles for obtaining SWC were measured at 447 locations, while soil core measurements (100 cm^3 sampling cylinders) were carried out at 152 locations, thereby increasing the spatial density of soil moisture observations. All sampling locations were accurately recorded using differential GPS (dGPS). In accordance with the procedures outlined by Heistermann et al. (2022), key soil properties were derived from oven-dried samples (105°C for 24 hours), ~~shown in Figure 8 (left). The objective of this study is twofold: firstly, to obtain time series of neutron count rate for each spectrometer sphere, and secondly, to provide unfolded neutron spectra that have been averaged over periods of several hourson different dates and times. Figure 8 (right)shows a time series for the neutron count rates of the spheres, indicating also the precipitation for the days of the measurements~~ including dry soil bulk density, soil water content, and organic matter as well as ~~four unfolded neutron spectra. The first pair of unfolded spectra was obtained from measurements taken prior to a precipitation event that occurred on~~ lattice water obtained from loss-on-ignition analysis (400°C for 16 hours and 1000°C for 12 ~~July 2025. The second pair of spectra was obtained two days after this event. The unfolded neutron spectra provide detailed information about the energy distributions of neutrons detected on site, as well as potential changes in the individual energy domains of the distributions. The unfolding solutions for both pairs of unfolded neutron spectra demonstrate stability both before and after the precipitation event. Furthermore, a change in the neutron distribution is evident before and after the precipitation event which can be attributed to the change of soil moisture in the area. The higher moderation of neutrons is attributable to the higher abundance of water (and its hydrogen atoms) in the soil following precipitation, resulting in a shift of neutron fluence from epithermal to thermal neutrons, while the high-energy part of the neutron distribution remain unchanged. This demonstrates the mechanism underlying the CRNS observation of water content via the detection of epithermal neutron intensities. Furthermore, it shows the potential of a BSS system to validate the neutron data time series measured with neighbouring CRNS detectors~~hours, respectively). Soil water content measurements taken manually with portable dielectric devices (ThetaProbe ML2x, Delta-T Devices LLC, Cambridge, UK) were individually corrected using a two-point (air–water) calibration for each device. The conversion from permittivity to SWC followed the equation of Zhao et al. (2016), with customized coefficients based on all PoSMO campaigns following Heistermann et al. (2022). This site-specific conversion, which yielded a root mean square error (RMSE) of ± 0.05 m^3 m^{-3} for the SWC estimates, was applied to all point-scale sensors – handheld and stationary.

To investigate the potential impact of tillage (by disc) on temporal variation of soil bulk density, a test in a plot cropped with maize was done in 2024. Bulk density was sampled at 0, 5, 10 and 15 cm before and again shortly after harvest and tillage, with a time difference of about 2 months.

~~– Left: Setup for the neutron measurements using the PTB extended range Bonner sphere spectrometer NEMUS-UMW. The individual Bonner spheres are encased in metal boxes to protect them from adverse weather conditions. Each sphere is suspended from springs to minimize noise due to vibrations. The boxes are distributed on a circle of radius of 3 meters, with the data logger and telemetry modules stored in a central box. The spheres are located 1.20 m above ground. Right: Neutron count rates of NEMUS-UMW system for different sphere sizes and thus neutron energy ranges (top figure), along with the precipitation records for the days of the measurements (bottom figure). Inlet graph in the top figure shows four unfolded neutron spectra corresponding to different days denoted in the inlet figure, two before and two after the precipitation event on 12 July 2025.~~

3.3 ~~Soil moisture~~ Continuous soil water content profiles at point scale

We employed four different methods for measuring ~~soil moisture~~ SWC profiles, each involving different depths and sensors (resulting in a total of 25 individual profiles, see Fig. 1, covering about two years of data~~, Fig. 1~~). This approach enabled us to capture detailed data on the vertical soil ~~moisture~~ water content dynamics relevant to infiltration and drying processes, which are vital for ~~extracting and understanding~~ improving the understanding of CRNS-derived soil ~~moisture~~ water content measurements (c.f. Scheiffele et al., 2020). The impedance-based profile probes (2 PR2/4 and 13 PR2/6, Delta-T Devices LLC, Cambridge, UK) collected data at 10, 20, 30, and 40 cm depths (with the PR2/6 extending to 60 and 100 cm). Five additional profiles each comprising 4–5 individual impedance-based probes (ThetaProbe ML2x, Delta-T Devices LLC, Cambridge, UK) extended the network by measuring at depths of up to 200 cm in areas where deeper monitoring was desirable or where profile probes were impractical to install. Furthermore, five soil ~~moisture~~ water content profiles were equipped with five TDR probes each (TDR100, Campbell Scientific Ltd., ~~UK~~Logan, USA) installed at depths of ~~9, 11,~~ 10, 25, 45, and 75 cm ~~. Measurements collected at 15-minute intervals were aggregated to hourly resolution. A two-point calibration (air, water)was applied for the impedance probes to adjust the raw sensor data. For converting permittivity values into volumetric soil moisturewe utilized the equation according to Zhao et al. (2016) with customized coefficients~~close proximity to the ATB climate station (Fig. 2). For all dielectric sensor we applied a site-specific conversion of measured permittivity to soil moisture, as described in ~~Heistermann et al. (2023).~~ section 3.2.

3.4 Shallow soil ~~moisture~~ water content from point-scale sensors

To enhance the monitoring of the upper soil layers at all CRNS stations ~~, additional~~ (e.g. for remote sensing applications), additional dielectric SMT100 sensors (Truebner, Germany) were installed at depths of 5 and 15 cm~~; via determining the oscillation frequency of a~~ . These time-domain ~~transmission system (Jackisch et al., 2020) they observe dielectric permittivity and also measure~~ transmission-based sensors (Jackisch et al., 2020) provide observations of soil water content and soil temperature. ~~The 5 cm measurement is closest to the surface soil moisture as observed by satellite remote sensing.~~ Shallower depths than ~~that~~ the chosen 5 cm are prone to larger errors in respect to ~~a realistic estimate of depth below a~~ deeper installation depths, considering the usually rough soil surface and the vertical averaging of soil moisture point-scale sensors such as the SMT100.

Thus, these observations constitute a cluster of soil moisture observation time series that provide a value close to the soil surface, give a difference (and gradient) in soil moisture for each time and furthermore could be linked to the soil moisture profiles recorded at the same locations but at different depths (section 3.3Measured permittivity was converted to SWC using a site-specific calibration function (section 3.2).

3.5 Campaign based soil moisture for CRNS calibration

Average soil dry bulk density (g cm^{-3}) in the top 30 cm of the soil, across the central area of the Potsdam Soil Moisture Observatory; the spatial distribution was obtained by Ordinary Kriging (exponential variogram with a range of 50 m).

3.5 Muon data

Neutron monitors, such as the the one at Jungfraujoch (JUNG), Switzerland, are conventionally used to correct locally measured epithermal neutron counts for variations in incoming neutrons. Recent studies suggest that local measurements of muon counts could improve this correction (Stevanato et al., 2022). Station #32 operated at PoSMO also includes muon detection (Gianessi et al., 2024), allowing for respective analyses. These data span January 2023 to July 2025 (see also Table 2).

To facilitate the calibration of the CRNS stations, a series of extensive field campaigns were conducted at 283 new profile locations, complemented by the data of two previous campaigns in 2019 and 2022 (Heistermann et al., 2023). This dataset encompasses a total of 38 campaigns within the CRNS cluster footprint, with both ThetaProbe and soil core measurements taken down to a depth of 35 cm. In total, the ThetaProbe profiles were conducted at 447 locations, while the soil core measurements were carried out at 152 locations, thereby increasing the spatial density of soil moisture observations. All sampling positions were accurately recorded using differential GPS (dGPS), and the bulk density distribution is depicted in Figure 7, revealing a relatively homogeneous site. To investigate the potential impact of agricultural practices, such as labor, on soil bulk density, a test in a plot with maize was done in 2024 to assess potential temporal changes by harvest and tillage (by disc) . Bulk density was sampled at 0,

3.6 Bonner sphere measurements of full neutron energy spectrum

Another option to potentially provide an estimate of the local incoming neutron flux are Bonner sphere spectrometers (ERBSS), as previously applied in combination with a temporary CRNS cluster (Fersch et al., 2020). Such measurements also yield background information on the neutron signal, for example, quantifying the thermal neutron component in the environment that must be eliminated prior to detection, as this contribution can impair the accurate counting of epithermal neutrons by CRNS devices.

Based on an existing ERBBS system, known as NEMUS (Wiegel and Alevra, 2002), Physikalisch-Technische Bundesanstalt (PTB) developed an SI-traceable version specifically for automated neutron spectrometry measurements under outdoor conditions (NEMUS-UMW), which was deployed at PoSMO during summer and autumn 2025. The system consists of a bare thermal neutron detector, 6 polyethylene spheres with diameters of 3, 4, 5, 6, 8 and 10 inches, and four modified spheres with lead and

copper shells, recording contributions from low to high neutron energies. The central detection of (thermal) neutrons inside the individual moderator sphere of each device was via spherical ^{3}He-filled proportional counters of type SP9 (Centronic Ltd., Croydon, UK), selected due to its low intrinsic background, which was systematically tested and quantified in a "neutron-free" environment (underground laboratory UDO II). Using unfolding procedures (Reginatto, 2010), the NEMUS response functions were characterized and validated in the PTB's neutron reference fields, and ~~15 cm before and after harvest and tillage events, with a time difference of about 2 months. The results gave no evidence that soil bulk density was different after harvest and tillage events than before, as a Tukeys-HSD test gave a p-value not being significant for rejecting the null hypothesis of being bulk densities being equal before and after. Soil bulk density was also determined specifically at 5 cm depth for ten of the cluster locations, including the more distant one to the East (#39), by taking horizontally cylinder rings of 100 cm^3 volume and measuring dry weight after drying in the oven at 105°C for 24 hours. Values ranged between 1.10 and 1.47 g cm^{-3} with a mean of 1.3 g cm^{-3} and standard deviation of 0.12 g cm^{-3}. In accordance with the procedures outlined by Heistermann et al. (2023) , key soil properties were derived from oven-dried samples, including dry soil bulk density and water content, as well as from loss-on-ignition analysis for organic matter content and lattice water. Additionally, manual soil moisture measurements were conducted using portable ThetaProbes, employing sensor-specific calibrations and a site-specific conversion of permittivity to soil moisture, resulting in a root mean square error (RMSE) of ± 0.05 m^3 m^{-3} for the soil moisture estimates~~thus the resulting unfolded neutron spectrum could be determined in absolute terms, i.e. neutron fluence $\Phi(E)$ in neutrons cm^{-2}.

3.7 Ground-based reference measurements of ~~Hyperspectral Surface Reflectance~~hyperspectral surface reflectance

~~The Hyperspectral Pointable System for Terrestrial and Aquatic Radiometry (HYPSTAR®) is a two-axis, autonomous hyperspectral radiometer designed to deliver multi-angular measurements of land and water surface reflectance . On~~ For measurements of ground-based hyperspectral surface reflectance on 11 October 2022, a HYPSTAR®-XR unit was installed at the ATB HYPERNETS site ~~at (~~close to CRNS station #11 (at 52°27′59.40" N, 12°57′35.16" E), mounted on a 5-meter mast with a 5-meter horizontal boom~~. The boom~~ , which was oriented southward toward a bare soil surface to avoid obstructions in the sensor's field of view. The ~~system acquires~~ Hyperspectral Pointable System for Terrestrial and Aquatic Radiometry (HYPSTAR®) is a two-axis, autonomous hyperspectral radiometer designed to deliver multi-angular measurements of land and water surface reflectance. The system acquired measurements every 30 minutes between 09:00 and 17:00 UTC across a range of zenith and azimuth angles ~~. It incorporates~~ until May 2024. It incorporated two spectrometers: a VNIR unit covering 380–1000 nm with 1,330 channels at 3 nm full width at half maximum (FWHM), and a SWIR unit covering 1000–1700 nm with 220 channels at 10 nm FWHM. An onboard camera ~~provides~~ provided contextual imagery, while an internal LED source ~~tracks~~ tracked calibration stability (De Vis et al., 2024; Goyens et al., 2021). Data ~~are~~ were transmitted to a central server and processed using the `hypernets_processor`, a Python-based pipeline for radiometric calibration, quality control, and computation of radiance, irradiance, and surface reflectance. The system rigorously propagates both random and systematic uncertainties, along with spectro-temporal covariance, ensuring that the data meet Fiducial Reference Measurement (FRM) standards (European Space Agency, 2024). The dataset collected ~~at the ATB Marquardt site~~ includes raw and processed surface reflectance data ~~. The data include~~ as a complete time series of angular hyperspectral surface reflectance for a bare soil target

under varying illumination and atmospheric conditions. ~~The dataset~~ It supports applications such as validation of radiative transfer models and soil spectral analysis. Future work ~~will~~ shall explore the use of this dataset for estimating surface soil moisture, using both empirical spectral indices and physically based retrieval approaches. The dataset provides also a valuable reference for validating airborne and satellite-based remote sensing products, to improve the retrieval accuracy of soil and vegetation parameters across scales. Additionally, it can support the development and calibration of radiative transfer and machine learning models for soil moisture, surface condition, and land-surface process monitoring.

3.8 Airborne hyperspectral data

Hyperspectral data were not only observed ~~as~~ at PoSMO as ground-based time series for a reference area ~~at the ATB Marquardt, within the Potsdam Soil Moisture Observatory, but accompanied by one time~~ (see section 3.7), but were accompanied by a dedicated airborne campaign on 5 September 2024~~providing hyperspectral and a~~ , providing hyperspectral as well as Lidar imagery. The former will be presented in this section, and the latter in the following section 3.9.

~~Airborne Hyperspectral Image Cube~~

Airborne hyperspectral data were acquired during an aerial survey campaign using two pushbroom imaging spectrometers ~~: the~~ mounted aboard a Cessna 208B Grand Caravan aircraft equipped with GNSS/IMU POS AV inertial navigation unit. These two sensors were a CASI-1500 (covering the visible to near-infrared range, VNIR: 380–1050 nm) and ~~the~~ a SASI-600 (covering the shortwave infrared range, SWIR: 950–2450 nm), both manufactured by Itres~~. The sensors were mounted aboard a Cessna 208B aircraft as part of an aerial survey campaign. The~~ , Calgary, Canada. The native spatial resolution achieved was 25 cm for CASI-1500 and 63 cm for SASI-600. The CASI sensor provided 15 spectral bands at an average spectral resolution of 38 nm, whereas SASI delivered 100 bands with a spectral resolution of 15 nm. The survey consisted of two parallel flight lines, each 375 m swath width~~, to ensure complete coverage of the designated test site~~.

~~Pre-Processing Workflow for airborne campaign~~

Initial data pre-processing was conducted by CZglobe (Czechglobe, the Czech Global Change Research Institute, Department of flight activities). Radiometric calibration was performed using the RadCorr software package, following the procedures outlined in Hanuš et al. (2023), and employed laboratory-derived sensor calibration parameters. Additional corrections included scattered light correction, frame shift smear correction, second-order light correction, and bad pixel interpolation to ensure optimal signal integrity. Georeferencing was accomplished using a GNSS/IMU navigation system in combination with a high-resolution digital terrain model (DTM), implemented within the GeoCor software suite. The hyperspectral imagery was projected into the UTM coordinate system (Zone 33N, ETRS-89 datum). Subsequent atmospheric correction and reflectance retrieval were carried out using ATCOR-4 (version 7.1) (Richter and Schläpfer, 2011)~~, developed by ReSe Applications in collaboration with DLR~~. The algorithm employs the MODTRAN radiative transfer model to correct for atmospheric effects and retrieve surface-level reflectance. The resulting reflectance values are stored as integer-scaled values, where a reflectance of 10.00 % is represented as 1000 (i.e., scaled by a factor of 100).

~~Coregistration and final data product for airborne hyperspectral imagery~~

Following atmospheric correction, the VNIR and SWIR datasets were spatially co-registered using the AROSICS software (Scheffler et al., 2017). The registration process utilized spectrally overlapping bands at 1004.8 nm (VNIR) and 1002.5 nm (SWIR) to ensure high alignment accuracy. The overall registration error could be reduced from an RMSE of 39 cm to 16 cm. Redundant overlapping bands were removed, and the SWIR data were resampled to match the finer spatial resolution of the CASI sensor (25 cm). The final dataset was generated by mosaicking the two flight lines and saved as Cloud Optimized GeoTIFF (COG), resulting in a geometrically and radiometrically consistent hyperspectral cube for subsequent analysis.

~~Illustration of the lidar data as a height colorized point cloud processed by open source tool CloudCompare, with focus on the central area of the CRNS cluster (14 of 16 stations included); view from South.~~

3.9 Airborne Lidar data

Airborne Lidar (ALS) data ~~was~~ were captured using a Riegl LMS Q-780 airborne full-waveform laser scanner mounted ~~onboard a CESSNA~~ also onboard the Cessna 208B ~~Grand Caravan equipped with GNSS/IMU POS AV inertial navigation unit~~(see section 3.8). The site was captured in three strips, north-south orientation, flown in the morning of ~~05/09/~~5 September 2024. The Riegl LMS Q-780 operates at a wavelength of 1064 nm with a laser pulse repetition rate of up to 400 kHz and a beam divergence of 0.25 mrad. FOV was 60°. Flight height was 620 m and scan line width was 710 m, 1190 m and 1660 m. The captured strips have an average point density of 7.3 points per m^2.

Strips were aligned using the RiPROCESS 1.9.2, RiUNITE, and GeoSysManager 2.2.4 software from RIEGL Laser Measurement System GmbH. For the flight trajectory calculations, the POSPac 8.7 software was used, followed by trajectory conversion in the Riegl-POFImport 1.8 software. ~~For processing in the RiPROCESS software it was necessary to convert the trajectory in POFImport to *.pofx format. In RiProcess~~ After import into the RiProcess software, the reference surfaces were first searched automatically. This was followed by the calculation of deviations between the same reference surfaces on different lines~~. The least squares method was used to minimize the deviations~~ , which then were minimized while adjusting the trajectory parameters for each individual flight line. The laser data was then re-georeferenced using the adjusted trajectories. The error (standard deviation) of the scan data adjustment was 0.007 m (based on 120.000 tie points). Data ~~was~~ were georeferenced to the ~~UTM33N (Universal Transverse Mercator - zone~~ UTM coordinate system (Zone 33N~~) coordinate system on ETRS-89 (European Terrestrial Reference System 1989~~, ETRS-89 datum). The resulting laser data ~~was~~ were exported as point clouds in ~~LAZ format~~ las-format (v1.4), including the so-called Riegl extra bytes, which associate ~~to each point~~ each point with the information from the full-waveform analysis (amplitude and pulse width). The ~~resulting point density~~ point density resulting is 15.2 points per m^2 in the co-registered point cloud.

~~On the processed data~~ Finally, noise was removed from the processed data using LAStools software, and a classification (surface and terrain) of the point cloud was performed. ~~A~~

As a result, a DTM (digital terrain model), DSM (digital surface model) and nDSM (normalized digital surface model – elevation map) are provided as individual Geotiff rasters with a spatial resolution of 0.25 m ~~. The provided lidar~~ (an example shown in Fig. 3). The provided Lidar dataset includes flight strip data (including amplitude, reflectance, pulse width) from the Riegl LMS Q-780 ~~as *.las as~~ in las-format as well as a mosaic of all co-registered *.laz lines and 1000 m x 1000 m tiles.

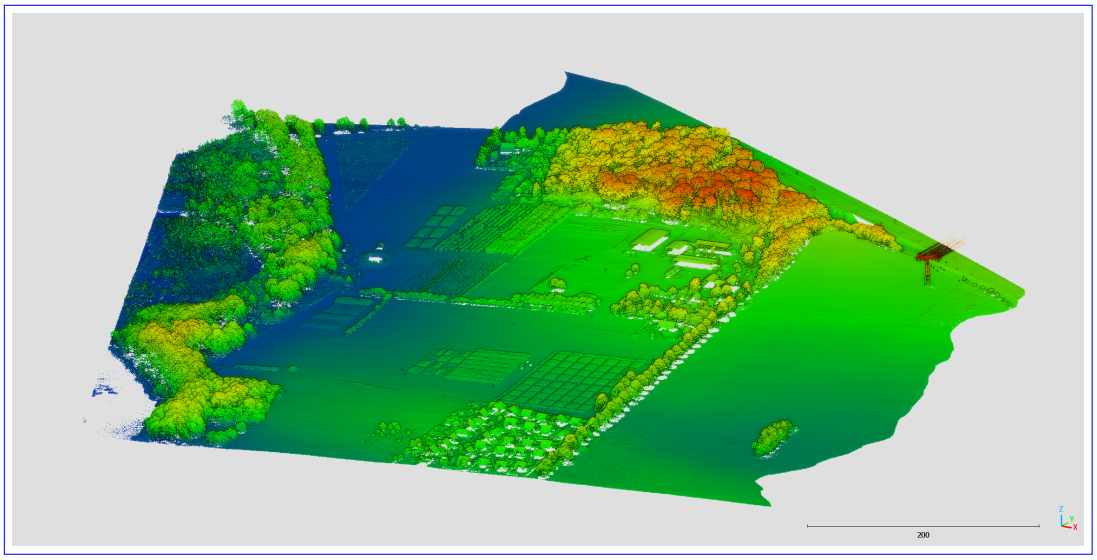

Figure 3. Illustration of the Lidar data as a height-colorized point cloud, with focus on the central area of PoSMO (14 of 16 stations included), retrieved on 5 September 2024; view from Southeast.

3.10 Land use, cropping and irrigation

The ~~thermal and epithermal~~ neutron counts recorded by ~~the CRNS detectors are highly sensitive to the vegetation. Remote sensing algorithms as well, also~~ CRNS are influenced by hydrogen contained in vegetation. Likewise, remote sensing algorithms require information on biomass ~~coverage~~ for calibration. To ~~facilitate~~ support a comprehensive comparison between remote sensing ~~data~~ products and CRNS measurements ~~, or to enable in-depth~~ and enable a more detailed analysis, we provide ~~additional information on crop distributions, types, and harvest values. This complementary dataset, provided~~ auxiliary information on crops grown (e.g., winter wheat, maize, alfalfa, sunflower) on the experimental plots at the fenced ATB site and the associated sowing and harvest dates. These data, supplied by the ATB~~(Leibniz-Institut für Agrartechnik und Bioökonomie),~~ ~~complete the airborne lidar data, and enables a more accurate assessment of the hydrogen pools. While no irrigation experiments were conducted during the study period, some~~ , complement the airborne Lidar dataset and improve the characterization of above-ground hydrogen pools for future CRNS analyses.

Several crops, including potatoes, maize, and spring wheat, received irrigation during ~~the summers of 2023 and 2024. Additionally, the~~ summer. The orchards (cherry~~and apple/strawberries/wines~~ , apple, strawberries, wine grape) and blueberry plantations were ~~regularly irrigated during the~~ also irrigated routinely during spring and summer~~months~~. All irrigation events ~~were recorded in the dataset~~ (plots, date, amount) are included in the dataset.

3.11 Snow cover campaign winter 2025

Snow cover at the research site is infrequent, with substantial continuous snow cover during several days typically occurring every 2-3 years. However, its occasional presence significantly influences the vertical soil water balance, and affects the interpretation of CRNS signals. Additionally, the surface's spectral characteristics are either completely masked or modified, making comprehensive documentation of snow cover periods ~~also~~ essential for remote sensing applications. ~~In mid-February~~ For the presented time span, three periods with persistent snow cover occurred: 16-21 January 2024, 10-14 January 2025, ~~few daysof persistent snow cover~~ and 13-21 February 2025 (end of periods +/- 0.5 days), each of them with a few centimeters of snow height. For the third period (mid-February 2025) with depths reaching a maximum of 6 cm~~occurred~~, a sampling campaign was conducted. We recorded ~~its temporal progression~~ the temporal progression of snow cover using a stationary wildlife camera (SECACAM HomeVista, VenTrade GmbH, Köln, Germany) capturing ~~hourly~~ images. The spatial distribution and properties of the respective snow cover were mapped using UAV-based RGB imagery with a Mavic Pro (Da-Jiang Innovations Science and Technology Co., Ltd, China) from ~~survey flights~~ a survey flight at 100 m flight altitude. The imagery was ~~stitched~~ mosaicked using Photoscan software (Agisoft LLC, St. Petersburg, Russia) and geo-referenced to 20 cm orthophotos provided by the Federal State of Brandenburg, producing an RGB image with ~~a~~ 3 cm ground resolution.

Additional manual snow sampling involved 240 measurements of snow depth ~~with~~ using a ruler and 10 ~~points for density measurements~~ density measurements obtained either through cylinder cores or by collecting all snow from a specific area for subsequent weighing in the field.

3.12 Groundwater and lake levels

Groundwater levels data complement soil moisture observations as they capture the subsurface response to recharge and storage changes, linking surface and vadose zone dynamics with aquifer behavior. The depth to the groundwater table at the western area of PoSMO increases from very shallow near the lake in the west towards approximately 10 m below ground in the east of the field site ~~. Groundwater during the operation of the PoSMO has~~ and water levels have been monitored in two wells along the slope ~~. Additionally~~ (see Fig. 2). Additionally, between September 2022 and January 2025 the lake level ~~(open water body of the Wublitz) was monitoredand is provided here~~was monitored. The upslope well is located in the vicinity of CRNS ~~sensor~~ station #22 approximately at the middle of the hillslope (ground elevation 36.17 m a.s.l.), the downslope well close to CRNS ~~sensor~~ station #2 (31.14 m a.s.l.) and the lake level is observed in a peripheral ditch in the vicinity of the same CRNS ~~sensor (Fig. 2).~~ station. The well pipes of 63 mm diameter have a length of 2 m, 4 m and 6 m for the lake, well ~~02 and well~~ #2 and well #22, respectively. They are ~~filtered~~ screened over a length of one meter at the lower end, and pressure sensors (Hobo U20L, Onset, Bourne, USA) were installed to record pressure and temperature at a 30 min interval. In well #22, an additional sensor recorded air pressure and temperature but had to be removed because of sensor failure in May 2024. To correct for air pressure variations after this time, air pressure recorded at the CRNS sensors were utilized. Regular manual measurements of the groundwater heads were used to validate the continuous measurements and exclude a drift in the pressure sensor measurements. Starting in September 2023, groundwater was pumped regularly for sampling stable water isotopes (see

section 3.13). The ~~resulting~~ periods with artificial drop in water table resulting from this sampling were excluded from the data set.

3.13 Stable water isotopes in soil and groundwater

Stable water isotopes (δ^2H and δ^{18}O) are widely used as natural tracers of water transport processes in the critical zone and across scales (Sprenger et al., 2019; Scandellari et al., 2024). Tracking the isotopic signature of precipitation through the soil profile enables qualitative and quantitative assessment of the timing and spatial variability of infiltration and percolation, and, together with soil moisture data, provides estimates of groundwater recharge (Canet-Martí et al., 2023; Wang et al., 2023; Koeniger et al., 2016). To qualitatively assess vertical percolation rates and their spatial heterogeneity within ~~the~~ PoSMO, we conducted three field campaigns under contrasting hydrological conditions. In May 2023, during dry soil conditions, profiles at locations #2 and #22 were sampled on 24 May, and at locations #21 and #11 on 26 May; groundwater was sampled subsequently on 31 May. No rainfall occurred between these dates, ensuring consistent conditions across sampling sites. In January 2024, following several days of snowfall and subsequent snowmelt, soil profiles at locations #2 and #22 were sampled on 25 January, and at #21 and #11 on 26 January, with groundwater sampled on the same day. In each campaign, bulk soil samples were collected along the hillslope at four ~~positions (~~locations (#2, #11, #21, and #22, see Fig. 2), covering the full soil depth from 0 to 150 cm at 10 cm intervals. To capture deeper infiltration of the January 2024 snowmelt, soil and groundwater samples were collected at all locations on 2 May 2024, and profiles at ~~positions~~ locations #21, #22, and #11 were extended to 200 cm for additional sampling.

Groundwater isotopes were analysed from piezometers at ~~positions~~ locations #2 and #22, with additional samples collected opportunistically between May 2024 and May 2025, generally about once per month.

During sampling, soil samples were sealed in Ziploc ~~®~~ bags (S. C. Johnson & Sons Inc., USA) to minimize evaporative losses and groundwater samples were stored in 10 ml vials. All samples were refrigerated until transport to the isotope laboratory of BOKU University in Vienna (Austria) for analysis of δ^2H and δ^{18}O ~~.~~

(Stumpp et al., 2018). In the laboratory, soil water isotopes were determined using the direct-equilibration method (Wassenaar et al., 2008). The isotopic ratios of the vapour of the soil samples as well as the isotopic ratios of the groundwater samples were determined using a Picarro L2130-i laser isotope analyser (Picarro Inc., Sunnyvale, ~~CA,~~ USA). The isotopic ratios of all samples are expressed in δ‰ units, which describe the relative difference in the ratio of heavy to light isotopes in a water sample with respect to VSMOW (Vienna Standard Mean Ocean Water). To better interpret the isotopic signature profiles of the water, the volumetric moisture content of the soil samples was also calculated. To do this, the gravimetric moisture of the samples was multiplied by ~~the bulk density of the soil~~ soil bulk density (ρ_b)~~. For ρ_b we took~~ , using average values by depth as measured earlier for these locations (Heistermann et al., 2023).

3.14 Soil saturated hydraulic conductivity in the root zone

Saturated hydraulic conductivity (K_{sat}) governs water flow through soil and controls key processes ~~like~~ such as infiltration, percolation and groundwater recharge~~. The spatial variability of soil properties, driven by heterogeneity in structure, texture,~~

and land use, makes , affecting both surface and subsurface hydrology. In unsaturated flow situations, K_{sat} difficult to measure directly in the field, so it is often derived in the laboratory or modelled (Durner, 1994; Hohenbrink et al., 2023). The PoSMO dataset overcomes this limitation by providing direct is also important, as it can be used in the estimation of unsaturated hydraulic conductivity curves (Durner, 1994; Hohenbrink et al., 2023). Due to spatial variability in soils, laboratory measurements on small soil cores often fail to represent field-scale conditions, a limitation highlighted in recent studies (Weber et al., 2024) . Field measurements of K_{sat}, by contrast, are considered to integrate over larger volumes, capturing effects of macropores and heterogeneities, and thus more accurately reflect the hydraulic response of natural soils (Reynolds et al., 2000). Because PoSMO targets larger-scale soil moisture and hydrological processes, we conducted field measurements of K_{sat} measurements at multiple depths and land uses, offering a more reliable basis for hydrological analyses. to assist in the assessment of water fluxes at the site.

K_{sat} was determined using a constant head permeameter (a so called amoozemeter*Amoozemeter*), which measures infiltration rates within an auger hole. During measurement, a constant hydraulic head was maintained in the hole while monitoring the infiltration rate until steady-state flow was achieved. K_{sat} was then calculated using the Glover equation (Amoozegar, 1989). A total of 28 measurements were conducted across different land uses, including grassland, orchards (cherry, berry, and apple trees), arable crops, and hazelnut hedges. Measurements were performed at depths of 12.5, 20 and 35 cm in eight soil profiles, with four of these profiles additionally sampled at 50 cm depth, following the methodology described by Elrick and Reynolds (1992). Data were collected between 6 January 2023 and 7 June 2024 under varying different wetness conditions. All K_{sat} estimates derived by this method represent the uppermost 50 cm of the soil column.

3.15 Electrical Resistivity Tomography (ERT) Surveys

Two Electrical Resistivity Tomography (ERT) surveys were conducted to provide a first overview of the deeper subsurface conditions at the core area of the Potsdam site. Results western area of PoSMO. The results can provide information about stratigraphic layering and inhomogeneities as well as the approximate groundwater table depth, helping to understand variations in surface soil moisture patterns. We used a Syscal ISIS system with 48 electrodes (IRIS Instruments, Orléans, France) along two perpendicular profiles: Profile 1 (A – A′) with 5 m electrode spacing (235 m total length) and Profile 2 (B – B') with 2.5 m spacing (117.5 m total length; see Figure Fig. 2) using a Wenner array. Electrode positions — including absolute elevations — were recorded with a Differential Global Position System (DGPSdGPS) antenna (Leica Zeno GG04, Leica Geosystems AG, Heerbrugg, Switzerland) for topographic correction of the resistivity data. The raw data sets from 16 November 2022 were imported and filtered in ProSys II (IRIS Instruments, Orléans, France). The apparent resistivity pseudo section was inverted in two dimensions using the open source GUI ResIPy (Blanchy et al., 2020) on a fine triangular mesh with convergence reached within two iterations. .

3.16 CRNS stations with long-term operation

Following the operation of the former, much A subset of PoSMO had been operated as a smaller CRNS cluster at the ATB site Marquardt (Heistermann et al., 2023), few since 2019 (Heistermann et al., 2023). Some of its CRNS stations were not

deinstalled and instead were integrated in the new clustersustained, shallow point sensors added and integrated as part of the newly established PoSMO design. These are CRNS with bold ID stations marked with bold IDs in Table 2, and the same holds for the accompanying SWC profile measurements. Thus, they provide a continuous these stations provide time series from 2019 to 2025, spanning the time frame of the old cluster (1 September 2019 to 30 November 2022), being part of the PoSMO (14 December 2023 to 31 July 2025) as well as the year between clusters. October 2025. For convenience of data users interested only in this longer term data set, they are provided here it is provided additionally as separate data files. The first three years of these time series are based on neutron counts and soil moisture profiles as provided Heistermann et al. (2023). The count rates and profile measurements as provided in Heistermann et al. (2023). These data together with the more recent data, as a complete neutron count time seriesis , were consistently processed, corrected and calibrated as the current data set described in 3.1.2 and for the soil moisture profile according to subsection 3.1.2 for CRNS and as described in section 3.3 for the SWC profiles.

4 External data

The subsections refers to following subsections describe datasets provided by third parties, either previously published or available through other channelssources. These datasets are relevant to interpret our data sets presented and thus are considered useful to readerssupport the interpretation of the data presented here and are therefore included for completeness and user reference.

4.1 DWD/ATB weather station

A climate station equipped with a heated tipping-bucket rain gauge is situated in the north-eastern part of the study areaATB site, as depicted in Fig.2. The station recorded 2. The station records standard climate variables at an hourly resolution, including air temperature, relative humidity, precipitation, soil temperature at multiple depths (5, 10, and 30 cm), and solar irradiation, as well as wind speed and direction. The original data are publicly accessible via the ATB website (ATB Technology Garden, 2025, last acce . This datasetprovides valuable information for understanding the climate conditions in the study area, and is an essential component of the overall dataset presented in this paper. The nearest climate station operated by the German Weather Service (DWD) is located at Telegrafenberg in Potsdam, approximately 12 km south-east (station ID 03987). The corresponding data are publicly available through DWD's open data repository (DWD, 2025) ()https://www2.atb-potsdam.de/Technologygarden/bsa_wetter.aspx. While not part of the primary dataset, this dataset offers valuable complementary information that may assist readers in interpreting the presented observations. The ATB operates another climate station at their main site in Potsdam-Bornim, located about 5 km south of PoSMO, and this data is also available online at https://www2.atb-potsdam.de/Technologygarden/atb_wetter.aspx. The nearest climate station operated by the German Weather Service (DWD) is located at Telegrafenberg in Potsdam, approximately 12 km south-east (station ID 03987). The corresponding data are publicly available through DWD's open data repository (DWD, 2025)(DWD, 2025).

4.2 Incoming Neutron Flux

The incoming cosmic-ray neutron flux is provided by the Neutron Monitor Database at http://www.nmdb.eu (last accessed on ~~01 July~~ 14 October 2025). In accordance with previous studies by Hawdon et al. (2014); Baatz et al. (2015); Jakobi et al. (2018); Baroni et al. (2018), the Jungfraujoch (JUNG) neutron monitor is recommended for correcting the incoming neutron flux at ~~the Potsdam site~~PoSMO. Recent approaches ~~include interpolation between different global neutron monitors~~ account more explicitly for the geomagnetic cut-off rigidity and shielding depth of the atmosphere at the measurement site in relation to different neutron monitors of the data base and promise to be more accurate ~~at locations in-between neutron monitors~~ (McJannet and Desilets, 2023).

4.3 Other spatial data and maps

A digital elevation model (DEM) with a resolution of 1 m × 1 m is available for download from the Landesvermessung und Geobasisinformation Brandenburg (LGB) website at https://geobroker.geobasis-bb.de~~(last accessed on 01 July 2025)~~, with an accuracy of 30 cm. Additionally, a soil map from the state of Brandenburg, BUEK300 (LBGR, 2025), provides soil types and texture data beyond the PoSMO area at a scale of 1:300 000 and is publicly accessible through the Brandenburg Geoportal at https://geoportal.brandenburg.de~~(last accessed on 01 July 2025)~~. For fieldwork and visualization purposes~~(Fig. 1)~~, we utilized OpenStreetMap data layers, which are available for download from the Geofabrik website at http://download.geofabrik.de~~(last accessed on 01 July 2025)~~. Specifically, we employed the land use, waterways, and traffic ways data layers~~, which provide valuable information for spatial analysis and visualization. Data~~ ; data are available under ODbL license ~~(~~http://www.openstreetmap.org/copyright).

~~5 CRNS-based soil moisture estimation~~

~~The period presented in the dataset spans from 14 December 2023 to 31 July 2025. For the data processing of CRNS neutron count time series the PYthon tool (Power et al., 2021a) was used. The raw neutron counts were filtered for any data points that deviated by more than 3 standard deviations (3σ) from the moving average. The neutron counts are influenced by atmospheric factors; therefore, we applied the following corrections: the effects of barometric pressure were corrected as well as the effects of incoming cosmic-ray neutron flux, using the station Jungfraujoch (Switzerland), following Zreda et al. (2012). Effects of atmospheric vapor content were corrected using the method described in Köhli et al. (2021). CRNS time series were calibrated using the transfer function from Desilets et al. (2010) with parameters a_0, a_1, and a_2, equal to 0.0808, 0.372, and 0.115, respectively. The estimation of soil moisture from neutron intensity was calibrated by using local soil moisture measurements in the sensor footprint, weighted following Schrön et al. (2017) 3.2. Resulting soil moisture time series are provided as hourly intervals and to reduce the statistical noise in CRNS data a 12-hour moving average (center) was applied.~~

~~To enhance sensor to sensor comparison, for example to process the neutron counts with a universal N_0 (Heistermann et al., 2024), detector sensitivities are provided (Table 2). The sensitivity of each detector was measured using a collocated calibrator probe~~

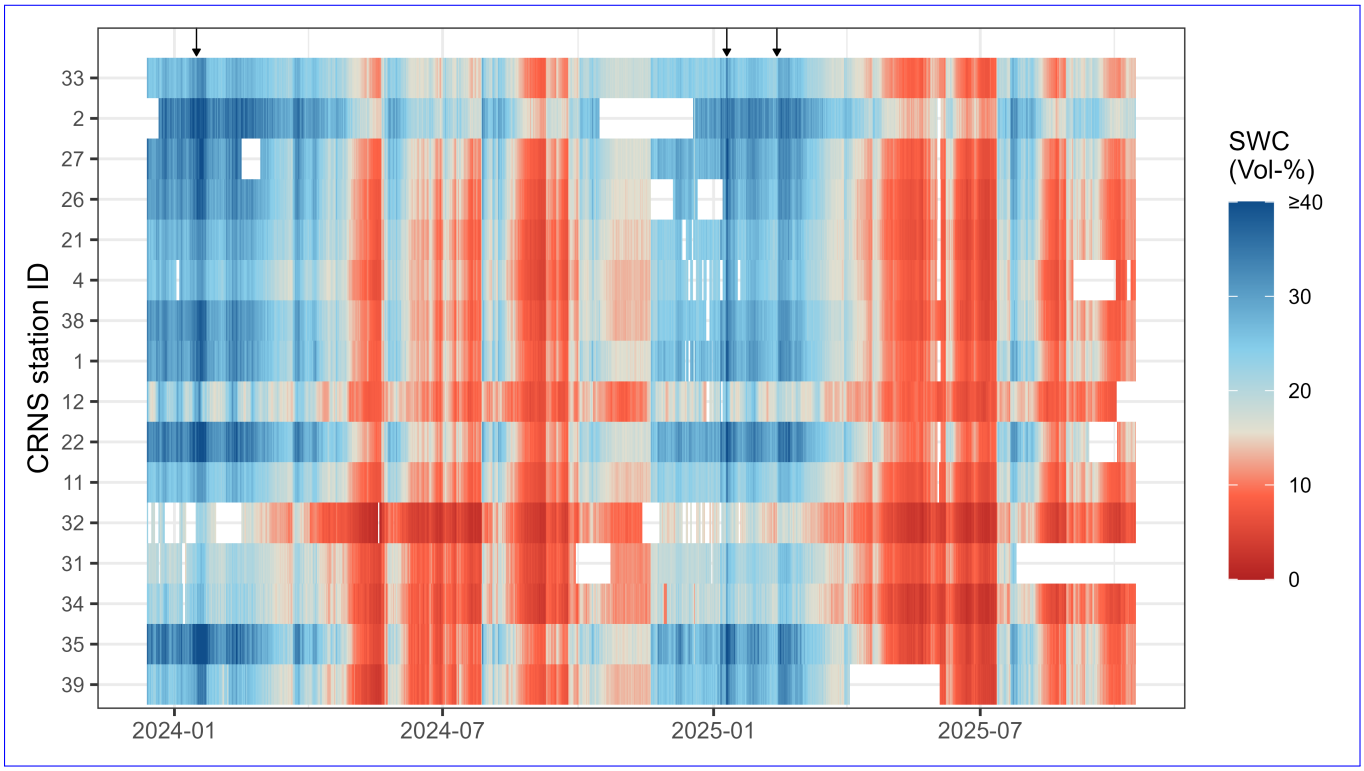

Figure 4. CRNS-derived daily SWC time series of PoSMO, arranged from west to east according to station positions. Arrows above the time series indicate periods of snow cover, which influence neutron counts and can lead to an apparent increase in retrieved soil water content.

~~or another CRNS sensor with known sensitivity, and the ratio of calibrator to stationary neutron counts was used to determine the sensitivity factor (Schrön et al., 2018).~~

5 Exemplary views of the data set

5.1 Examples of CRNS-derived root-zone soil moisture

6 ~~Summary use cases for the data~~

The data set presented and described here can contribute to understand soil moisture spatial patterns ~~at landscape scale~~ and related soil moisture dynamics ~~, especially in the first~~ at the plot- to landscape-scale, especially within the top decimeters of soil. ~~But the design of PoSMO~~ However, the merit of the PoSMO data goes beyond that, as ~~it closes~~ these data close the spatial gap between point observations ~~, -~~ or even soil moisture in-situ networks ~~, -~~ and larger scale observations and ~~modelling~~modeling. In particular~~satellite -~~, remote sensing can use the data as reference for soil moisture related products, ~~while being different to the usual sites~~ because they provide especially high representativity compared to other mixed-land use

reference sites used for calibration and validation~~(cal-val)~~. For this purpose, PoSMO was established at the km~~scale (which is also a ^{2}-scale~~ (which corresponds to the typical resolution of current hydrological or also land-surface models). Thus, ~~several~~ suitable grid cells of remote sensing products or distributed land surface models could be ~~directly~~ adequately compared, assimilated or used for validation, as has been done with stand-alone CRNS already ~~(e.g., Baatz et al., 2017; Fatima et al., 2024a).~~ (e.g., Baatz et al., 2017; Fatima et al., 2024b). Figure 4 presents a comprehensive overview of the SWC time series data from December 2023 to October 2025. The temporal dynamics of the 16 locations exhibit consistent patterns over time, but also differences in SWC across the site are evident in respect to absolute values as well as dynamics. As a simple way of ordering, the CRNS stations have been listed according to their position, from west to east. This heat map reveals five major dry spells (occurring in summer 2024 and summer 2025, with CRNS soil moisture below 15 % for all stations) and long wet conditions during winter including one snow cover period in January 2024 and two snow cover periods in January to February 2025 (see also section 3.11).

~~PoSMO provides ready-to-use~~

Figure 5 illustrates the soil moisture dynamics of CRNS sensors and dielectric sensors as a response to rainfall, exemplarily for July 2024 and July 2025. Inherent to the non-invasive measurement the effective integration depth (D86) of CRNS-sensors varies to some degree with soil water content, for these two summer months between about 20 and 40 cm, and stays around 30 cm as mean across the CRNS cluster (panel (c)), while CRNS-derived SWC values ranged between about 5 and 25 % . The D86-estimate presented here is derived from the independently measured point-scale SWC profiles (all sensing depths) rather than from CRNS-derived SWC alone. The depth weighting procedure for point-scale data is described in detail by Schrön et al. (2017) and involves an iterative estimation of point-scale average SWC, effective sensing depth D86 and CRNS apparent soil moisture (see their section 2.3). By explicitly accounting for the shape of the SWC profile (and all sensing depths), our approach addresses an an important control on CRNS-derived soil moisture estimates (Baroni et al., 2018), which is not captured when relying solely on CRNS-derived soil moisture values (cf. Appendix A in Schrön et al. (2017)). Due to small-scale heterogeneity and uncertainty in quantitative estimates from the dielectric sensors, however, the daily estimate of the integration depth based on a single soil water content profile might not be fully representative for the respective CRNS footprint. During the full time frame and accross all PoSMO stations, the effective integration depth estimates varied between 15 and 46 cm (on average 25 cm). This illustrates the representativeness of CRNS for root-zone soil moisture (RZSM). While the overall dynamics of the CRNS-derived SWC time series is most comparable to those of the 5 and 10 cm soil layers (Fig. 5), the CRNS measurements have a higher responsiveness to small rainfall inputs, as CRNS is also detecting water content in the soil layers shallower than 5 cm, which cannot reliably be captured with point-scale sensors. Additionally, the range of absolute values of both CRNS- and dielectric sensors for any given time suggests that there is considerable spatial heterogeneity, which calls for spatially aggregating measurement methods such as CRNS. A fair an direct comparison between CRNS-derived and point-scale SWC can be achieved either by vertically "unweighting" the CRNS data, to make it comparable to a depth-averaged soil moisture profile (Scheiffele et al., 2020), or by applying depth scaling methods such as the exponential filter (Franz et al., 2020; Rasche et al., 2024), which can interpolate the different soil moisture data to the same nominal depths.

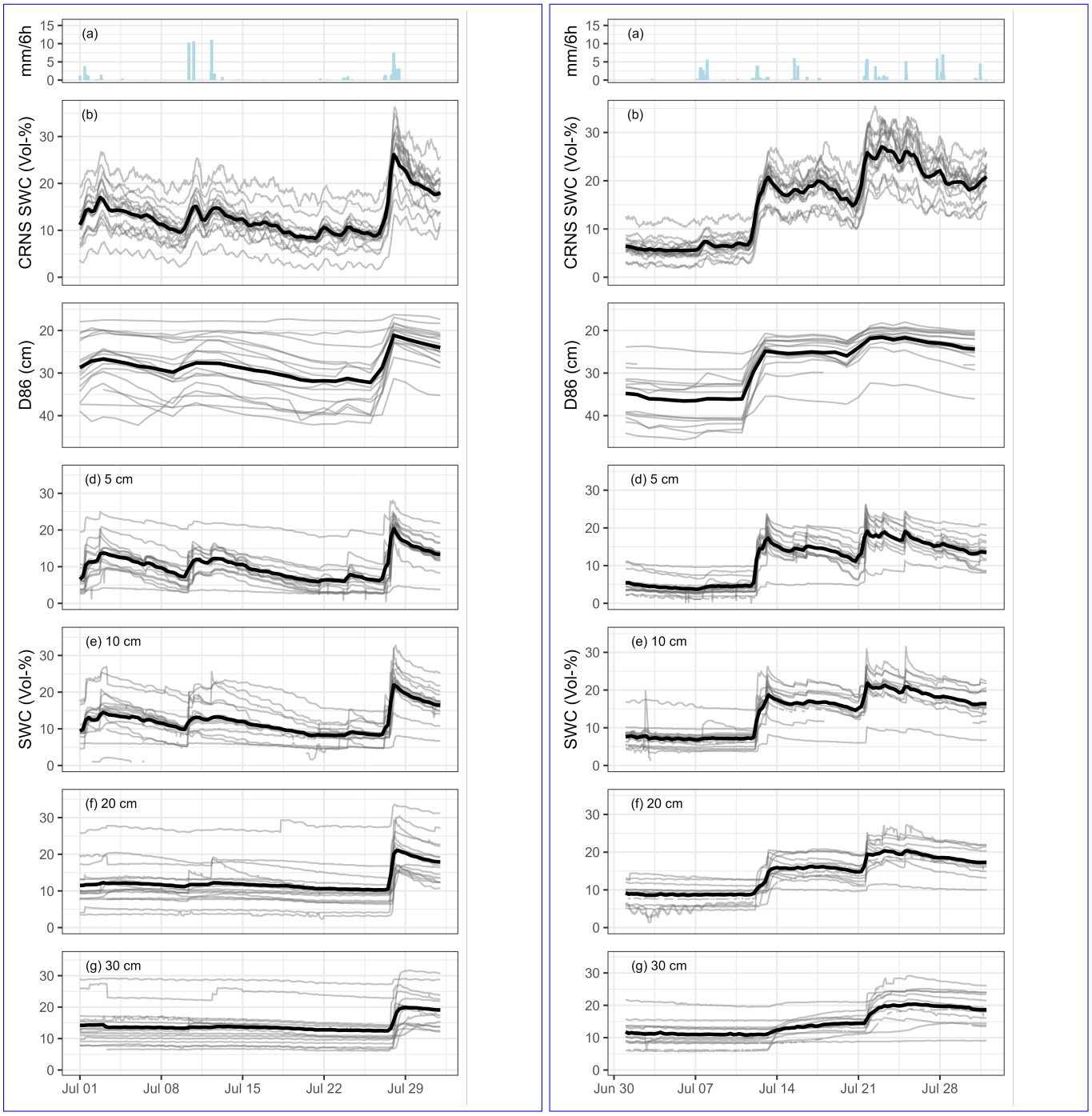

Figure 5. Exemplary view of soil moisture dynamics in July 2024 and July 2025. (a) Precipitation amount in mm/6h from DWD climate station in Potsdam, (b) CRNS-derived soil water content representing RZSM (with a 6 hour moving average) (c) Estimated daily D86-integration depth of CRNS observation based on the independently measured point-scale soil water content profiles (d) – (g) soil water content derived from point-scale dielectric sensors at 5 to 30 cm depth. Grey lines are measurements at individual stations, the bold line represents the arithmetic mean of the whole sensor cluster.

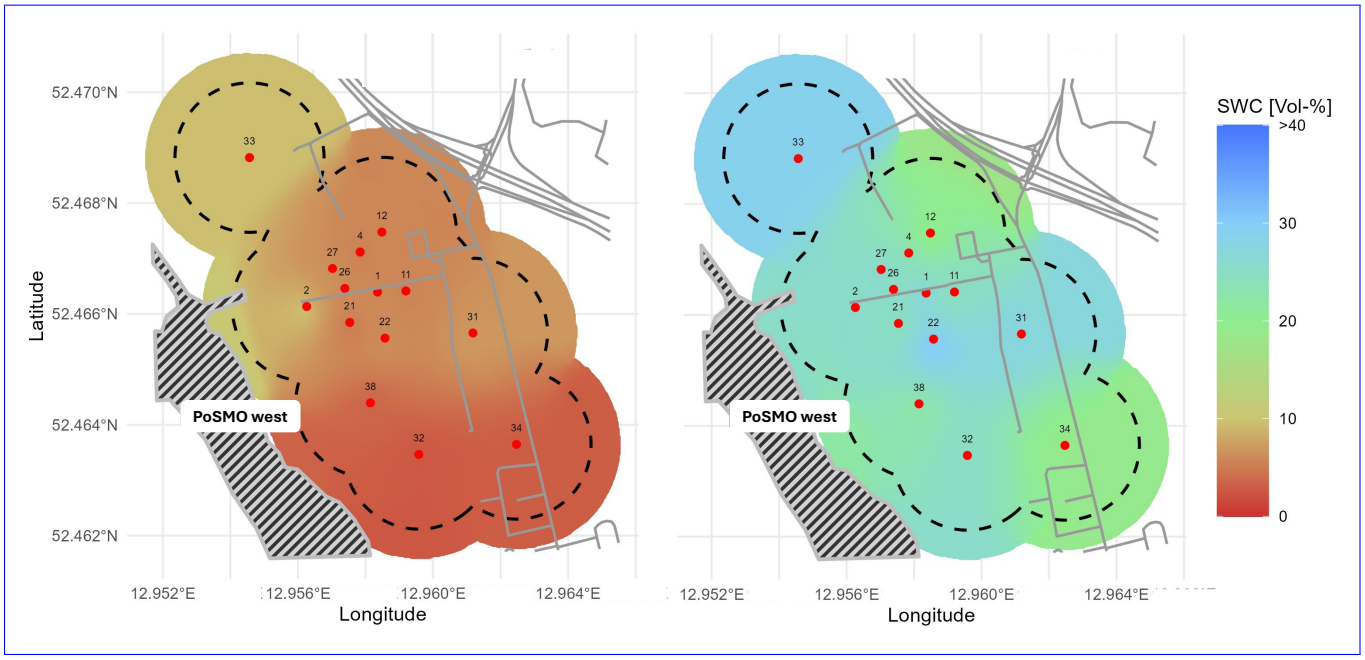

Figure 6. Root-zone soil moisture maps from CRNS-derived soil water content (SWC) attributed to the CRNS station locations in the western area of PoSMO (cf. section 3.1.1), shown for a day during a dry period in September 2024 (left) and for a relatively moist day after autumn rewetting in November 2024 (right). Dashed circles illustrate the area circumference covered, based on a 150 m footprint radius for each CRNS sensor. SWC was interpolated onto a 2 m grid (details see text). Map background information see Fig. 2.

The spatial distribution of CRNS soil moisture is shown exemplarily in Fig. 6 for 8 September 2024 and 24 November 2024 during relatively dry and moist conditions, respectively. Spatial interpolation on a 2 m grid shows an initial impression of the soil moisture distribution for specific days. For this visualization only, inverse distance weighting was applied, treating each CRNS station as a point measurement. However, due to the large horizontal footprint of CRNS, more robust interpolation approaches should account for the sensors' horizontal sensitivity, as demonstrated in Heistermann et al. (2021).

Soil moisture estimates derived from CRNS data are susceptible to several sources of uncertainty, including corrections on neutron counts and the influence of hydrogen contained in vegetation. These effects are only implicitly included in the soil moisture product provided here through the local calibration procedure (sections 3.1.2 and 3.2). Consequently, the soil moisture product presented in this dataset should be regarded as an estimate that can be further refined as correction approaches advance. For example, the most recent method for correcting the incoming neutron flux by McJannet and Desilets (2023) scales the dynamics of the neutron monitor time series to the theoretical dynamics at the CRNS site using the geomagnetic cut-off rigidity and shielding depth of the atmosphere. This approach has been shown to outperform earlier methods by Zreda et al. (2012) and Hawdon et al. (2014), as demonstrated in Schrön et al. (2024); Hertle et al. (2025); McJannet et al. (2025). Likewise, a more explicit consideration of biomass and its temporal dynamics could reduce biases and improve the robustness of CRNS soil water content estimates (Jakobi et al., 2022), and recent research suggests that combined measurements of epithermal

and thermal neutron detectors may even allow biomass estimation (Brogi et al., 2025). Nevertheless, the CRNS-derived soil moisture provided here constitutes a valid and representative estimate of root-zone soil moisture, including the most dynamic soil-plant-atmosphere interactions (root density typically highest within the upper 40 cm of the soil profile (Schenk and Jackson, 2002)) and thus the zone of strongest temporal variability in soil moisture and water fluxes.

5.1 Examples subsurface properties

Soil bulk density information is important for calibrating dielectric soil moisture sensors and within the functions to transfer neutrons to soil moisture (section 3.2). Extensive measurement efforts at the experimental site allowed to generate interpolated maps of bulk density distribution for the top soil layer, as shown in Fig. 7 (panel a), revealing some local variations across the site, though larger parts have similar values.

A small case study assessed the impact of agricultural practices on temporal variation of bulk density by sampling soil before and after harvest at one of the larger agricultural fields. No significant effect was detected: bulk density did not differ significantly before and after harvest or tillage (Tukey's test, $\alpha = 0.05$). Given the absence of detectable temporal changes, all measurements were merged into a single dataset. Based on 152 soil cores, bulk density values ranged from 1.10 to 1.47 $\mathrm{g\,cm^{-3}}$, with a mean of 1.30 $\mathrm{g\,cm^{-3}}$ and a standard deviation of 0.12 $\mathrm{g\,cm^{-3}}$.

Figure 7 (panel b) shows the first results of the ERT survey at the field site (see section 3.15 and locations of cross sections in Fig. 2). The zones of highest electrical conductivity shown in the inverted pseudsections approximately coincided with the depth of the groundwater table, as indicated from the monitoring wells (section 3.12). Inferring deeper soil water storage from conductivity patterns would require time-lapse ERT measurements and/or higher-resolution shallow surveys, combined with independent calibration using profile soil moisture data.

5.2 Examples neutron spectrometer

Since 18 June 2025, the ERBSS system has been operated at PoSMO close to CRNS station #31 until 04 December 2025. We obtained time series of neutron intensities for different energies, and are able to provide daily neutron spectra. Figure 8 shows time series for the neutron count rates of the individual detector spheres, indicating also daily precipitation and highlighting neutron spectra for four particular days. The first two were obtained on 8 and 9 July 2025, prior to a precipitation event around 12 July 2025, and the other two on 14 and 15 July 2025, after about 30 mm of cumulated rain has been received. The resulting neutron spectra provide detailed information about the energy distributions of neutrons detected on site. The character of the neutron spectrum is the same before and after the precipitation event, but there occurred a decrease of neutron fluence in the epithermal and fast range, while the high-energy parts of the neutron distribution, i.e. the incoming neutron intensity, remained unchanged. This change in the neutron distribution induced by the precipitation event can be attributed to the increase of soil water content in the first decimeters of soil (cf. Fig. 5, right graph). This reflects the mechanism underlying the CRNS observation of root-zone soil moisture via the detection of epithermal neutron intensities. Furthermore, it demonstrates the potential of an ERBSS system to characterize the incoming neutron component and a future development of a local, observation-based incoming correction.

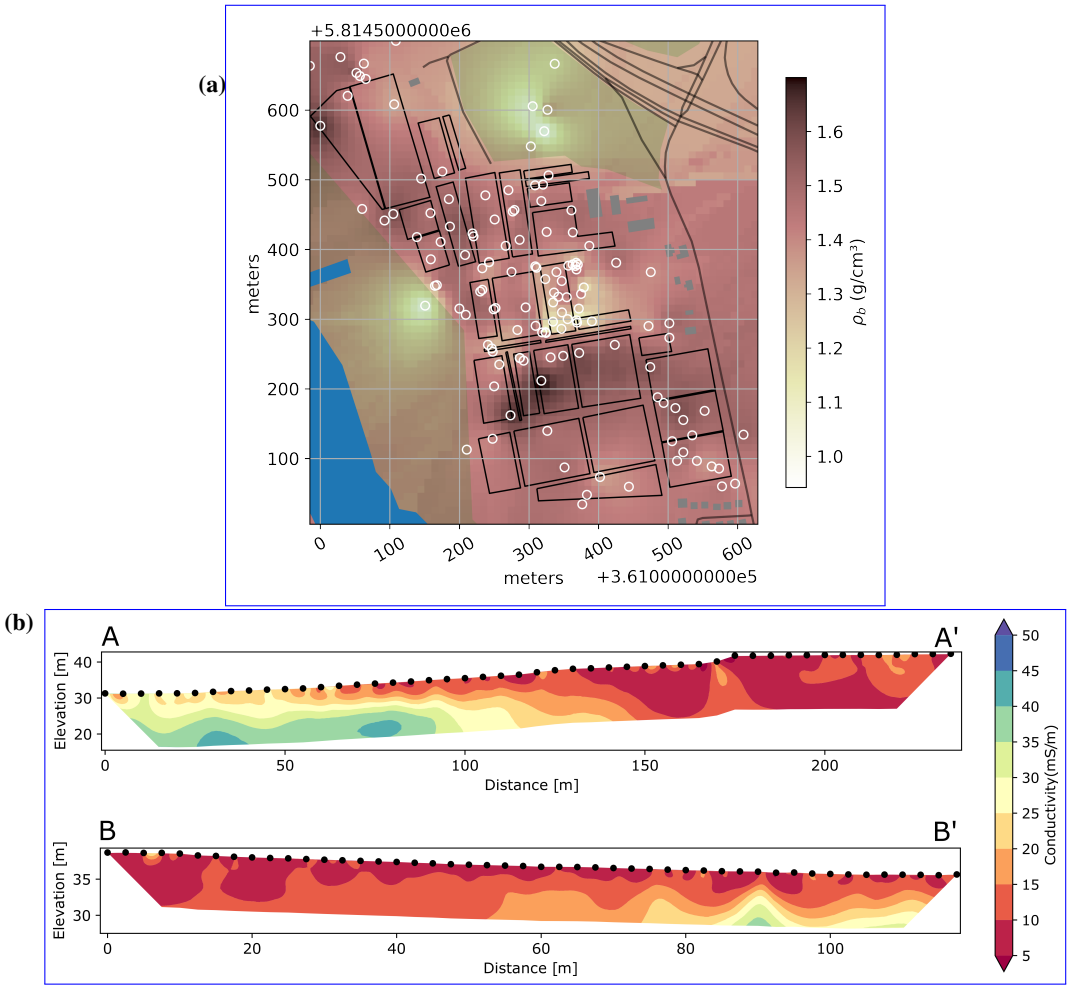

Figure 7. (a) Average soil dry bulk density (g cm^{-3}) in the top 30 cm of the soil, across the western area of the Potsdam Soil Moisture Observatory; the spatial distribution was obtained by Ordinary Kriging (exponential variogram with a range of 50 m). (b) ERT profiles of electrical conductivity in two transects at the hillslope part of PoSMO (A–A' from west to east, B–B' from north to south, see Fig. 2).

5.3 Examples remote sensing

PoSMO provides carefully compiled, high-resolution SWC time series~~which will facilitate~~, including standardized metadata and documentation. This dataset facilitates the cross-validation and uncertainty ~~quantification~~ assessment of the increasing number of high resolution (e.g. 1 km) SWC products ~~coming from downscaling~~ derived from downscaled coarse-resolution ~~RS microwave sources and reanalysis dataor RS~~ remote sensing microwave sources or reanalysis data, as well as from active microwave sources (Fan et al., 2025).

As an example, ~~Figure~~ Fig. 9, on the left, shows the Copernicus SWI product (~~soil water index)derived from S-1~~ Soil Water Index), derived from Sentinel-1 constellation covering the Potsdam Observatory. The Copernicus surface soil moisture

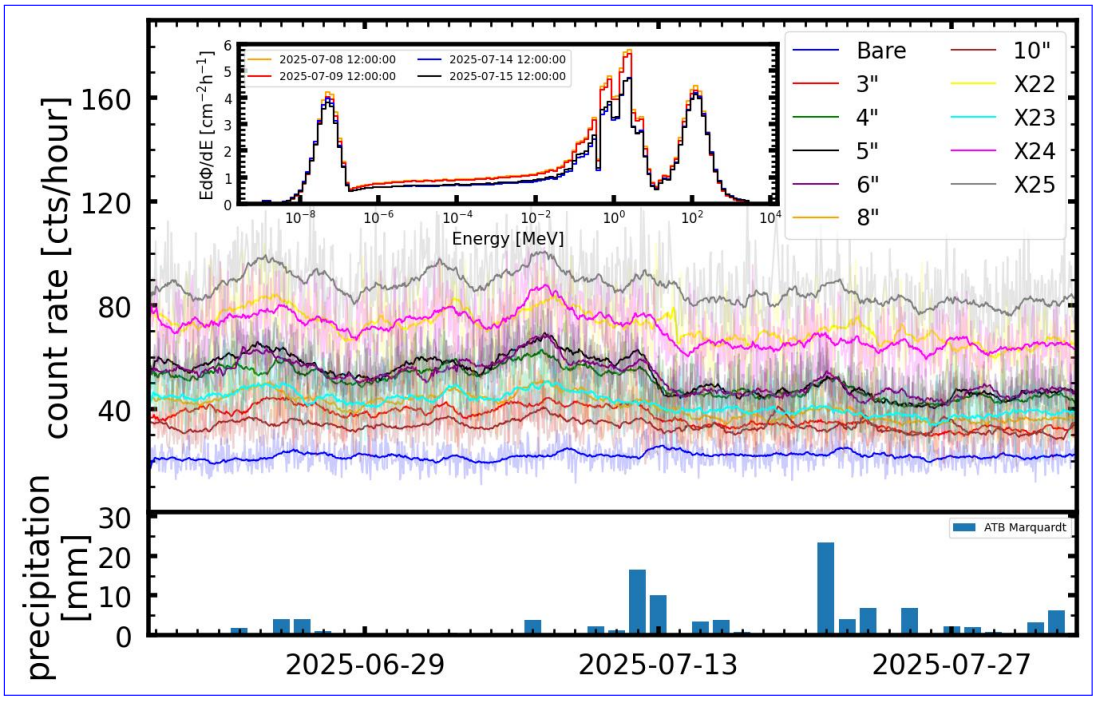

Figure 8. Neutron count rates of the ERBSS system for different sphere sizes (moderators) and thus neutron energy ranges (top panel), along with the precipitation records at the site (bottom panel). Inlet graph in the top panel shows exemplarily unfolded neutron spectra on two days before and two days after the rain event on 12 and 13 July 2025, as recorded on site.

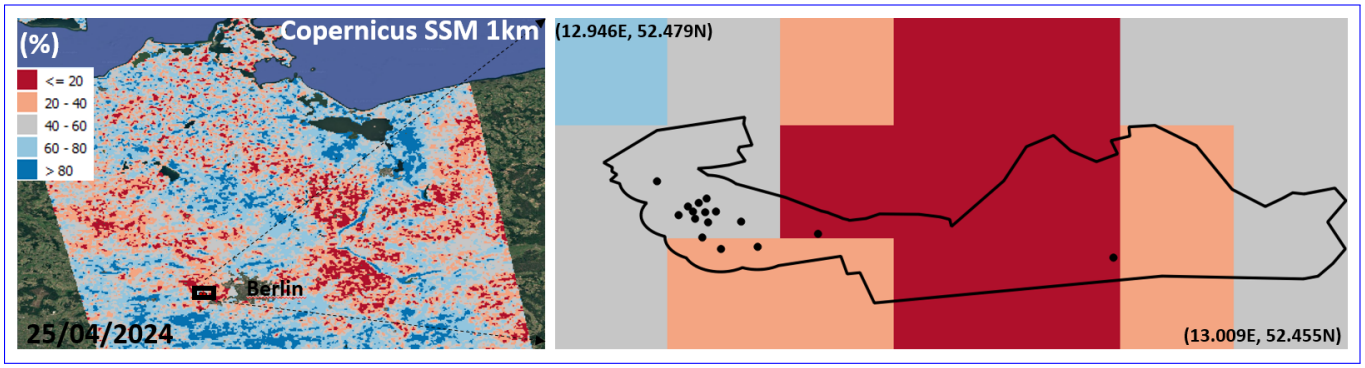

Figure 9. Left: Example of Copernicus Sentinel-1 relative Surface Soil Moisture (SSM), in % saturation for Northern Germany on 25 April 2024 (left). Zoom into the PoSMO area, with dots indicating an individual cluster location with CRNS, SMT100 and soil moisture profile each (right); pixel size is 1 by 1 km; the black outline marks area of similar land use and soil type, as represented by PoSMO (see Fig. 1).

product represents an index of saturation that can be converted into volumetric water content by multiplying it by the soil porosity. On the right, the figure zooms in on the ~~cluster locationswith respect to the Copernicus SWI~~ PoSMO locations,

highlighting the product's 1 km pixels. The ~~higher support~~ larger support volume of each CRNS ~~and the dense number of CRNS distributed in the area of~~ together with the relatively dense distribution of CRNS within the 3.4 km^2 ~~will enable an extensive comparison between RS~~ area of similar land use and soil type, enhances comparisons between remote sensing products and reference SWC ~~measurements, minimizing the spatial representativeness uncertainty~~ data. Although the clustered layout does not provide uniform spatial coverage, the multi-sensor information helps reduce local sampling uncertainty and improves the overall representativeness of the ground ~~data~~observations for validation.

~~Left: Example of Copernicus SWI on 25 April 2024. Right: Zoom into the PoSMO area, with dots indicating an individual cluster location with CRNS, SMT100s and soil moisture profile each. The stations data can be flexibly aggregated and directly assigned to a particular remote sensing pixel, if desired as reference data.~~

6 Conclusions

~~The extensive supplementary data accompanying the soil moisture observations provide the context needed to interpret their spatial and temporal dynamics within a broader hydrological framework, linking them to controlling variables such as soil properties(e.g. saturated hydraulic conductivity or bulk density), as well as supporting the interpretation of water fluxes from~~ In conclusion, the Potsdam Soil Moisture Observatory (PoSMO) dataset provides a unique, multi-scale and long-term record of soil water dynamics under agricultural management. By combining CRNS-based soil moisture, profile and shallow in-situ measurements, groundwater observations, hydraulic and physical soil properties, stable water isotopes~~and groundwater data, or exploiting hyperspectral imagery to assess vegetation traits, soil characteristics, and surface conditions~~, and complementary remote sensing and hyperspectral information, the dataset offers a comprehensive basis for hydrological process studies and for the development, calibration, and validation of large-scale soil moisture products. The spatial density, temporal continuity, and multidisciplinary character of this dataset make it a robust reference for hydrological research, such as studies of land–atmosphere exchange or drought monitoring, and for transferring insights to comparable lowland agricultural regions.

7 Data availability

For data archiving, we utilized EUDAT (https://eudat.eu). The data resides on the ~~B2share server ()~~ B2Share server at https://doi.org/10.23728/b2share.bxamy-4zh85 (Grosse et al., 2025). Its structure corresponds to the subsections of section 3 of this paper. Each data subset is accompanied by a metadata text file (JSON format), offering additional details on the data format, units, column descriptors and remarks.

Author contributions. SO, PG, TF, LS, MH, and KDP designed the study and coordinated the instrumentation; PG, EM, and TF coordinated the data management; PG and EM coordinated and led the writing of the manuscript. LS, PG, and SO led the revision of the manuscript; PG was responsible for setting up and maintaining the instrumentation; MeSch assisted with data analysis; BT co-designed the instrument network and provided data on land use, yields and irrigation water use; CN and DS contributed the airborne hyperspectral imagery, MeSa the

hyperspectral ground-based time series and MK the airborne Lidar imagery; KDP did experimental work in the field in respect to stable water isotope data and together with CS the laboratory isotope analyses; DR provided soil moisture profiles from TDRs; MZ, JM, SR conceived the Bonner sphere set-up and performed the measurements with help of PG; DA performed the ERT measurements and LS added the preliminary analysis; SO headed the PoSMO effort and is the principal investigator of this study; all authors contributed by writing particular parts of the manuscript.

Competing interests. No conflict of interest to declare.

Acknowledgements. This research was funded by the Deutsche Forschungsgemeinschaft (DFG, German Research Foundation) – research unit FOR 2694 "Cosmic Sense", project number 357874777, and project SoMMet that has received funding from the European Partnership on Metrology (Funder name: European Partnership on Metrology, Funder ID: 10.13039/100019599, Grant number: 21GRD08 SoMMet), co-financed from the European Union's Horizon Europe Research and Innovation Programme and by the Participating States.

We thank the Helmholtz-Centre for Environmental Research - UFZ, Leipzig, for providing the majority of CRNS detectors deployed in ~~this cluster~~the Potsdam Soil Moisture Observatory. Furthermore, we acknowledge the help of our technician Peter Bíró, Marie-Therese Schmehl and student workers for assistance in field work and data preparation: ~~Isabel von Boetticher,~~ Paola Aleman Serrano, Jakob Terschlüßen, Isabel von Boetticher, Milan Flügel; and project work by Sebastian Rothermel. Out thanks also goes to the EWP-Stadtwerke Potsdam GmbH for allowing us to set up a CRNS network location on their premises in Satzkorn outside the ATB site. The measurements with a hyperspectral airborne sensor ~~was~~ were partly based on use of Large Research Infrastructure CzeCOS supported by the Ministry of Education, Youth and Sports of CR within the CzeCOS program, grant number LM2023048. And we acknowledge the NMDB database www.nmdb.eu, founded under the European Union's FP7 programme (contract no. 213007), for providing data from their JUNG measurements at Jungfraujoch, Switzerland.

References

Abioye, E. A., Abidin, M. S. Z., Mahmud, M. S. A., Buyamin, S., Ishak, M. H. I., Rahman, M. K. I. A., Otuoze, A. O., Onotu, P., and Ramli, M. S. A.: A Review on Monitoring and Advanced Control Strategies for Precision Irrigation, Computers and Electronics in Agriculture, 173, 105 441, https://doi.org/10.1016/j.compag.2020.105441, 2020.

Amoozegar, A.: Comparison of the Glover Solution with the Simultaneous-Equations Approach for Measuring Hydraulic Conductivity, Soil Science Society of America Journal, 53, 1362–1367, https://doi.org/10.2136/sssaj1989.03615995005300050010x, 1989.

Arnault, J., Fersch, B., Schrön, M., Bogena, H. R., Franssen, H.-J. H., and Kunstmann, H.: Role of Infiltration on Land–Atmosphere Feedbacks in Central Europe: Fully Coupled WRF-Hydro Simulations Evaluated with Cosmic-Ray Neutron Soil Moisture Measurements, Journal of Hydrometeorology, 26, 129–153, https://doi.org/10.1175/JHM-D-24-0049.1, 2025.

ATB Technology Garden: ATB Weather, TechnologyGarden Marquardt (Leibniz-Institut Für Agrartechnik Und Bioökonomie e.V.), https://www2.atb-potsdam.de/Technologygarden/bsa_wetter.aspx, 2025.

Baatz, R., Bogena, H. R., Hendricks-Franssen, H.-J., Huisman, J. A., Montzka, C., and Vereecken, H.: An empirical vegetation correction for soil water content quantification using cosmic ray probes, Water Resour. Res., 51, 2030–2046, https://doi.org/10.1002/2014wr016443, 2015.

Baatz, R., Franssen, H.-J. H., Han, X., Hoar, T., Bogena, H. R., and Vereecken, H.: Evaluation of a cosmic-ray neutron sensor network for improved land surface model prediction, Hydrol. Earth Syst. Sc., 21, 2509–2530, https://doi.org/10.5194/hess-21-2509-2017, 2017.

Babaeian, E., Sadeghi, M., Franz, T. E., Jones, S., and Tuller, M.: Mapping soil moisture with the OPtical TRApezoid Model (OPTRAM) based on long-term MODIS observations, Remote Sens. Environ., 211, 425–440, https://doi.org/10.1016/j.rse.2018.04.029, 2018.

Barbosa, L. R., Coelho, V. H. R., Scheiffele, L. M., Baroni, G., Filho, G. M. R., Montenegro, S. M., das N. Almeida, C., and Oswald, S. E.: Dynamic groundwater recharge simulations based on cosmic-ray neutron sensing in a tropical wet experimental basin, Vadose Zone J., e20145, https://doi.org/10.1002/vzj2.20145, 2021.

Baroni, G. and Oswald, S.: A scaling approach for the assessment of biomass changes and rainfall interception using cosmic-ray neutron sensing, J. Hydrol., 525, 264–276, https://doi.org/10.1016/j.jhydrol.2015.03.053, 2015.

Baroni, G., Scheiffele, L. M., Schrön, M., Ingwersen, J., and Oswald, S. E.: Uncertainty, sensitivity and improvements in soil moisture estimation with cosmic-ray neutron sensing, J. Hydrol., 564, 873–887, https://doi.org/10.1016/j.jhydrol.2018.07.053, 2018.

Bauer-Marschallinger, B., Freeman, V., Cao, S., Paulik, C., Schaufler, S., Stachl, T., Modanesi, S., Massari, C., Ciabatta, L., Brocca, L., and Wagner, W.: Toward Global Soil Moisture Monitoring With Sentinel-1: Harnessing Assets and Overcoming Obstacles, IEEE Transactions on Geoscience and Remote Sensing, 57, 520–539, https://doi.org/10.1109/TGRS.2018.2858004, 2019.

Beale, J., Waine, T., Evans, J., and Corstanje, R.: A Method to Assess the Performance of SAR-Derived Surface Soil Moisture Products, IEEE Journal of Selected Topics in Applied Earth Observations and Remote Sensing, 14, 4504–4516, https://doi.org/10.1109/JSTARS.2021.3071380, 2021.

Blanchy, G., Saneiyan, S., Boyd, J., McLachlan, P., and Binley, A.: ResIPy, an Intuitive Open Source Software for Complex Geoelectrical Inversion/Modeling, Computers & Geosciences, 137, 104 423, https://doi.org/10.1016/j.cageo.2020.104423, 2020.

Bogena, H. R., Herrmann, F., Jakobi, J., Brogi, C., Ilias, A., Huisman, J. A., Panagopoulos, A., and Pisinaras, V.: Monitoring of Snowpack Dynamics With Cosmic-Ray Neutron Probes: A Comparison of Four Conversion Methods, Frontiers in Water, Volume 2 - 2020, https://doi.org/10.3389/frwa.2020.00019, 2020.

Bogena, H. R., Schrön, M., Jakobi, J., Ney, P., Zacharias, S., Andreasen, M., Baatz, R., Boorman, D., Duygu, M. B., Eguibar-Galán, M. A., Fersch, B., Franke, T., Geris, J., González Sanchis, M., Kerr, Y., Korf, T., Mengistu, Z., Mialon, A., Nasta, P., Nitychoruk, J., Pisinaras, V., Rasche, D., Rosolem, R., Said, H., Schattan, P., Zreda, M., Achleitner, S., Albentosa-Hernández, E., Akyürek, Z., Blume, T., del Campo, A., Canone, D., Dimitrova-Petrova, K., Evans, J. G., Ferraris, S., Frances, F., Gisolo, D., Güntner, A., Herrmann, F., Iwema, J., Jensen, K. H., Kunstmann, H., Lidón, A., Looms, M. C., Oswald, S., Panagopoulos, A., Patil, A., Power, D., Rebmann, C., Romano, N., Scheiffele, L., Seneviratne, S., Weltin, G., and Vereecken, H.: COSMOS-Europe: a European network of cosmic-ray neutron soil moisture sensors, Earth System Science Data, 14, 1125–1151, https://doi.org/10.5194/essd-14-1125-2022, 2022.

Bojinski, S., Verstraete, M., Peterson, T. C., Richter, C., Simmons, A., and Zemp, M.: The Concept of Essential Climate Variables in Support of Climate Research, Applications, and Policy, Bulletin of the American Meteorological Society, 95, 1431–1443, https://doi.org/10.1175/BAMS-D-13-00047.1, 2014.

Brocca, L., Ciabatta, L., Massari, C., Camici, S., and Tarpanelli, A.: Soil Moisture for Hydrological Applications: Open Questions and New Opportunities, Water, 9, 140, https://doi.org/10.3390/w9020140, 2017.

Brogi, C., Bogena, H. R., Koehli, M., Huisman, J. A., Franssen, H.-J. H., and Dombrowski, O.: Feasibility of irrigation monitoring with cosmic-ray neutron sensors, Goescientific Instrumentation Methods and Data Systems, 11, 451–469, https://doi.org/10.5194/gi-11-451-2022, 2022.

Brogi, C., Jakobi, J., Huisman, J. A., Schmidt, M., Montzka, C., Bates, J. S., Akter, S., and Bogena, H. R.: Cosmic-Ray Neutron Sensors Provide Scale-Appropriate Soil Water Content and Vegetation Observations for Eddy Covariance Stations in Agricultural Ecosystems, Agricultural and Forest Meteorology, 373, 110 731, https://doi.org/10.1016/j.agrformet.2025.110731, 2025.

Canet-Martí, A., Morales-Santos, A., Nolz, R., Langergraber, G., and Stumpp, C.: Quantification of water fluxes and soil water balance in agricultural fields under different tillage and irrigation systems using water stable isotopes, Soil and Tillage Research, 231, 105 732, https://doi.org/10.1016/j.still.2023.105732, 2023.

Cooper, H. M., Bennett, E., Blake, J., Blyth, E., Boorman, D., Cooper, E., Evans, J., Fry, M., Jenkins, A., Morrison, R., Rylett, D., Stanley, S., Szczykulska, M., Trill, E., Antoniou, V., Askquith-Ellis, A., Ball, L., Brooks, M., Clarke, M. A., Cowan, N., Cumming, A., Farrand, P., Hitt, O., Lord, W., Scarlett, P., Swain, O., Thornton, J., Warwick, A., and Winterbourn, B.: COSMOS-UK: national soil moisture and hydrometeorology data for environmental science research, Earth Syst. Sci. Data, 13, 1737–1757, https://doi.org/10.5194/essd-13-1737-2021, 2021.

De Vis, A., Goyens, C., Gaultier, L., Giardino, C., Vansteenwegen, J., Harpole, S., and Sterckx, S.: HYPERNETS: An autonomous, uncertainty-quantified reference network for validating satellite-derived surface reflectance over land and water, Frontiers in Remote Sensing, 5, 1347 230, https://doi.org/10.3389/frsen.2024.1347230, 2024.

Denager, T., Looms, M. C., Sonnenborg, T. O., and Jensen, K. H.: Comparison of Evapotranspiration Estimates Using the Water Balance and the Eddy Covariance Methods, Vadose Zone Journal, 19, e20 032, https://doi.org/10.1002/vzj2.20032, 2020.

Desilets, D., Zreda, M., and Ferré, T. P. A.: Nature's neutron probe: Land surface hydrology at an elusive scale with cosmic rays, Water Resources Research, 46, https://doi.org/https://doi.org/10.1029/2009WR008726, 2010.

Dorigo, W. A., Himmelbauer, I., Aberer, D., Schremmer, L., Petrakovic, I., Zappa, L., Preimesberger, W., Xaver, A., Annor, F., Ardö, J., Baldocchi, D., Bitelli, M., Blöschl, G., Bogena, H., Brocca, L., Calvet, J.-C., Camarero, J. J., Capello, G., Choi, M., Cosh, M. C., van de Giesen, N., Hajdu, I., Ikonen, J., Jensen, K. H., Kanniah, K. D., de Kat, I., Kirchengast, G., Kumar Rai, P., Kyrouac, J., Larson, K., Liu, S., Loew, A., Moghaddam, M., Martínez Fernández, J., Mattar Bader, C., Morbidelli, R., Musial, J. P., Osenga, E., Palecki, M. A., Pellarin, T., Petropoulos, G. P., Pfeil, I., Powers, J., Robock, A., Rüdiger, C., Rummel, U., Strobel, M., Su, Z., Sullivan, R., Tagesson, T., Varlagin,

A., Vreugdenhil, M., Walker, J., Wen, J., Wenger, F., Wigneron, J. P., Woods, M., Yang, K., Zeng, Y., Zhang, X., Zreda, M., Dietrich, S., Gruber, A., van Oevelen, P., Wagner, W., Scipal, K., Drusch, M., and Sabia, R.: The International Soil Moisture Network: Serving Earth System Science for over a Decade, Hydrology and Earth System Sciences, 25, 5749–5804, https://doi.org/10.5194/hess-25-5749-2021, 2021.

Durner, W.: Hydraulic Conductivity Estimation for Soils with Heterogeneous Pore Structure, Water Resources Research, 30, 211–223, https://doi.org/10.1029/93WR02676, 1994.

DWD: CDC (Climate Data Center) Deutscher Wetterdienst, https://opendata.dwd.de/climate_environment/CDC/observations_germany/climate/hourly/, 2025.

Elrick, D. E. and Reynolds, W. D.: Methods for analyzing constant-head well permeameter data, Soil Science Society of America Journal, 56, 320–323, https://doi.org/10.2136/sssaj1992.03615995005600010052x, 1992.

Entekhabi, D., Njoku, E. G., O'Neill, P. E., Kellogg, K. H., Crow, W. T., Edelstein, W. N., Entin, J. K., Goodman, S. D., Jackson, T. J., Johnson, J., Kimball, J., Piepmeier, J. R., Koster, R. D., Martin, N., McDonald, K. C., Moghaddam, M., Moran, S., Reichle, R., Shi, J. C., Spencer, M. W., Thurman, S. W., Tsang, L., and Van Zyl, J.: The Soil Moisture Active Passive (SMAP) Mission, Proceedings of the IEEE, 98, 704–716, https://doi.org/10.1109/JPROC.2010.2043918, 2010.

European Space Agency: Fiducial Reference Measurements for Soil Moisture (FRM4SM): Executive Summary Report, Tech. Rep. ESA Contract No. 4000135204/21/I-BG, European Space Agency, Paris, France, https://earth.esa.int/eogateway/documents/d/earth-online/frm4sm_executive_summary_report_v2-0, [Accessed 21 Nov 2025]. Prepared by AWST, CESBIO, TU Wien., 2024.

Fan, D., Zhao, T., Jiang, X., García-García, A., Schmidt, T., Samaniego, L., Attinger, S., Wu, H., Jiang, Y., Shi, J., Fan, L., Tang, B.-H., Wagner, W., Dorigo, W., Gruber, A., Mattia, F., Balenzano, A., Brocca, L., Jagdhuber, T., Wigneron, J.-P., Montzka, C., and Peng, J.: A Sentinel-1 SAR-based global 1-km resolution soil moisture data product: Algorithm and preliminary assessment, Remote Sensing of Environment, 318, 114 579, https://doi.org/10.1016/j.rse.2024.114579, 2025.

Fatima, E., Kumar, R., Attinger, S., Kaluza, M., Rakovec, O., Rebmann, C., Rosolem, R., Oswald, S., Samaniego, L., Zacharias, S., and Schrön, M.: Improved representation of soil moisture simulations through incorporation of cosmic-ray neutron count measurements in a large-scale hydrologic model, Hydrol. Earth Syst. Sc., 2024, 1–33, https://doi.org/10.5194/egusphere-2023-1548, preprint, 2024a.

Fatima, E., Kumar, R., Attinger, S., Kaluza, M., Rakovec, O., Rebmann, C., Rosolem, R., Oswald, S. E., Samaniego, L., Zacharias, S., and Schrön, M.: Improved representation of soil moisture processes through incorporation of cosmic-ray neutron count measurements in a large-scale hydrologic model, Hydrology and Earth System Sciences, 28, 5419–5441, https://doi.org/10.5194/hess-28-5419-2024, 2024b.

Fatima, E., Kumar, R., Altdorff, D., Attinger, S., Boeing, F., Oswald, S. E., Rakovec, O., Samaniego, L., Zacharias, S., and Schrön, M.: On the value of mobile cosmic-ray neutron measurements for spatio-temporal soil moisture simulations, Frontiers in Water, Volume 7 - 2025, https://doi.org/10.3389/frwa.2025.1630051, 2025.

Fersch, B., Francke, T., Heistermann, M., Schrön, M., Döpper, V., Jakobi, J., Baroni, G., Blume, T., Bogena, H. R., Budach, C., Gränzig, T., Förster, M., Güntner, A., Hendricks-Franssen, H.-J., Kasner, M., Köhli, M., Kleinschmit, B., Kunstmann, H., Patil, A., Rasche, D., Scheiffele, L., Schmidt, U., Szulc-Seyfried, S., Weimar, J., Zacharias, S., Zreda, M., Heber, B., Kiese, R., Mares, V., Mollenhauer, H., Völksch, I., and Oswald, S. E.: A dense network of cosmic-ray neutron sensors for soil moisture observation in a highly instrumented pre-Alpine headwater catchment in Germany, Earth Syst. Sci. Data, 12, 2289–2309, https://doi.org/10.5194/essd-12-2289-2020, 2020.

Foolad, F., Franz, T. E., Wang, T., Gibson, J., Kilic, A., Allen, R. G., and Suyker, A.: Feasibility Analysis of Using Inverse Modeling for Estimating Field-Scale Evapotranspiration in Maize and Soybean Fields from Soil Water Content Monitoring Networks, Hydrology and Earth System Sciences, 21, 1263–1277, https://doi.org/10.5194/hess-21-1263-2017, 2017.

Franz, T. E., Wahbi, A., Zhang, J., Vreugdenhil, M., Heng, L., Dercon, G., Strauss, P., Brocca, L., and Wagner, W.: Practical Data Products From Cosmic-Ray Neutron Sensing for Hydrological Applications, Front. Water, 2, 1–9, https://doi.org/10.3389/frwa.2020.00009, 2020.

Gianessi, S., Polo, M., Stevanato, L., Lunardon, M., Francke, T., Oswald, S. E., Said Ahmed, H., Toloza, A., Weltin, G., Dercon, G., Fulajtar, E., Heng, L., and Baroni, G.: Testing a novel sensor design to jointly measure cosmic-ray neutrons, muons and gamma rays for non-invasive soil moisture estimation, Geoscientific Instrumentation, Methods and Data Systems, 13, 9–25, https://doi.org/10.5194/gi-13-9-2024, 2024.

Gorelick, N., Hancher, M., Dixon, M., Ilyushchenko, S., Thau, D., and Moore, R.: Google Earth Engine: Planetary-scale geospatial analysis for everyone, Remote Sensing of Environment, https://doi.org/10.1016/j.rse.2017.06.031, 2017.

Goyens, C., De Vis, A., Giardino, C., Harpole, S., and Sterckx, S.: The HYPERNETS Project: A New Hyperspectral Radiometer and Network for Satellite Validation, in: 2021 IEEE International Geoscience and Remote Sensing Symposium IGARSS, pp. 1117–1120, https://doi.org/10.1109/IGARSS47720.2021.9553361, 2021.

Grosse, P. M., Marret, E., Scheiffele, L., Dimitrova Petrova, K., Francke, T., Altdorff, D., Heistermann, M., Schiel, M., Neumann, C., Scheffler, D., Saberioon, M., Kunz, M., Zboril, M., Marach, J., Reginatto, M., Balenzano, A., Stumpp, C., Trost, B., and Oswald, S. E.: The Potsdam Soil Moisture Observatory: High-coverage reference observations at kilometer scale, b2share EUDAT [data set], https://doi.org/10.23728/b2share.bxamy-4zh85, 2025.

Gruber, A., De Lannoy, G., Albergel, C., Al-Yaari, A., Brocca, L., Calvet, J.-C., Colliander, A., Cosh, M., Crow, W., Dorigo, W., Draper, C., Hirschi, M., Kerr, Y., Konings, A., Lahoz, W., McColl, K., Montzka, C., Muñoz-Sabater, J., Peng, J., Reichle, R., Richaume, P., Rüdiger, C., Scanlon, T., van der Schalie, R., Wigneron, J.-P., and Wagner, W.: Validation practices for satellite soil moisture retrievals: What are (the) errors?, Remote Sensing of Environment, 244, 111 806, https://doi.org/https://doi.org/10.1016/j.rse.2020.111806, 2020.

Hanuš, J., Slezák, L., Fabiánek, T., Fajmon, L., Hanousek, T., Janoutová, R., Kopkáně, D., Novotný, J., Pavelka, K., Pikl, M., Zemek, F., and Homolová, L.: Flying Laboratory of Imaging Systems: Fusion of Airborne Hyperspectral and Laser Scanning for Ecosystem Research, Remote Sensing, https://doi.org/10.3390/rs15123130, 2023.

Hawdon, A., McJannet, D., and Wallace, J.: Calibration and correction procedures for cosmic-ray neutron soil moisture probes located across Australia, Water Resources Research, 50, 5029–5043, https://doi.org/10.1002/2013WR015138, 2014.

Heistermann, M., Francke, T., Schrön, M., and Oswald, S. E.: Spatio-temporal soil moisture retrieval at the catchment scale using a dense network of cosmic-ray neutron sensors, Hydrol. Earth Syst. Sc., 25, 4807–4824, https://doi.org/10.5194/hess-25-4807-2021, 2021.

Heistermann, M., Bogena, H., Francke, T., Güntner, A., Jakobi, J., Rasche, D., Schrön, M., Döpper, V., Fersch, B., Groh, J., Patil, A., Pütz, T., Reich, M., Zacharias, S., Zengerle, C., and Oswald, S.: Soil moisture observation in a forested headwater catchment: combining a dense cosmic-ray neutron sensor network with roving and hydrogravimetry at the TERENO site Wüstebach, Earth System Science Data, 14, 2501–2519, https://doi.org/10.5194/essd-14-2501-2022, 2022.

Heistermann, M., Francke, T., Scheiffele, L., Dimitrova Petrova, K., Budach, C., Schrön, M., Trost, B., Rasche, D., Güntner, A., Döpper, V., Förster, M., Köhli, M., Angermann, L., Antonoglou, N., Zude-Sasse, M., and Oswald, S. E.: Three years of soil moisture observations by a dense cosmic-ray neutron sensing cluster at an agricultural research site in north-east Germany, Earth System Science Data, 15, 3243–3262, https://doi.org/10.5194/essd-15-3243-2023, 2023.

Heistermann, M., Francke, T., Schrön, M., and Oswald, S. E.: Technical Note: Revisiting the general calibration of cosmic-ray neutron sensors to estimate soil water content, Hydrol. Earth Syst. Sc., 28, 989–1000, https://doi.org/10.5194/hess-28-989-2024, 2024.

Hertle, L., Zacharias, S., Larsen, N., Rasche, D., McJannet, D., and Schrön, M.: Neutron Monitor Based Incoming Flux Correction for Cosmic-Ray Neutron Sensing of Environmental Water, Water Resources Research, 61, e2025WR040 527, https://doi.org/10.1029/2025WR040527, 2025.

Hohenbrink, T. L., Jackisch, C., Durner, W., Germer, K., Iden, S. C., Kreiselmeier, J., Leuther, F., Metzger, J. C., Naseri, M., and Peters, A.: Soil water retention and hydraulic conductivity measured in a wide saturation range, Earth System Science Data, 15, 4417–4432, https://doi.org/10.5194/essd-15-4417-2023, 2023.

Hövel, A., Stumpp, C., Bogena, H., Lücke, A., Strauss, P., Blöschl, G., and Stockinger, M.: Hydro-Meteorological Drivers of Event Runoff Characteristics Under Analogous Soil Moisture Patterns in Three Small-Scale Headwater Catchments, Hydrological Processes, 39, e70 173, https://doi.org/10.1002/hyp.70173, 2025.

Jackisch, C., Germer, K., Graeff, T., Andrä, I., Schulz, K., Schiedung, M., Haller-Jans, J., Schneider, J., Jaquemotte, J., Helmer, P., Lotz, L., Bauer, A., Hahn, I., Šanda, M., Kumpan, M., Dorner, J., de Rooij, G., Wessel-Bothe, S., Kottmann, L., Schittenhelm, S., and Durner, W.: Soil moisture and matric potential – an open field comparison of sensor systems, Earth System Science Data, 12, 683–697, https://doi.org/10.5194/essd-12-683-2020, 2020.

Jakobi, J., Huisman, J. A., Vereecken, H., Diekkruger, B., and Bogena, H. R.: Cosmic Ray Neutron Sensing for Simultaneous Soil Water Content and Biomass Quantification in Drought Conditions, Water Resour. Res., 54, 7383–7402, https://doi.org/10.1029/2018wr022692, 2018.

Jakobi, J., Huisman, J. A., Fuchs, H., Vereecken, H., and Bogena, H. R.: Potential of Thermal Neutrons to Correct Cosmic-Ray Neutron Soil Moisture Content Measurements for Dynamic Biomass Effects, Water Resour. Res., 58, e2022WR031 972, https://doi.org/10.1029/2022WR031972, 2022.

Kerr, Y., Waldteufel, P., Wigneron, J.-P., Martinuzzi, J., Font, J., and Berger, M.: Soil moisture retrieval from space: the Soil Moisture and Ocean Salinity (SMOS) mission, IEEE Transactions on Geoscience and Remote Sensing, 39, 1729–1735, https://doi.org/10.1109/36.942551, 2001.

Koeniger, P., Gaj, M., Beyer, M., and Himmelsbach, T.: Review on soil water isotope-based groundwater recharge estimations, Hydrological Processes, 30, 2817–2834, https://doi.org/10.1002/hyp.10775, 2016.

Köhli, M., Schrön, M., Zreda, M., Schmidt, U., Dietrich, P., and Zacharias, S.: Footprint Characteristics Revised for Field-Scale Soil Moisture Monitoring with Cosmic-Ray Neutrons, Water Resources Research, 51, 5772–5790, https://doi.org/10.1002/2015WR017169, 2015.

Köhli, M., Weimar, J., Schrön, M., Baatz, R., and Schmidt, U.: Soil Moisture and Air Humidity Dependence of the Above-Ground Cosmic-Ray Neutron Intensity, Frontiers in Water, 2, https://doi.org/10.3389/frwa.2020.544847, 2021.

Krebs, N., Schattan, P., Premier, V., Mejia-Aguilar, A., Fey, C., Bremer, M., and Rutzinger, M.: Evaluating Sentinel-1/-2 and MODIS fractional snow cover products for applications in alpine cosmic ray neutron snow monitoring, Remote Sensing Applications: Society and Environment, 40, 101 812, https://doi.org/https://doi.org/10.1016/j.rsase.2025.101812, 2025.

Köhli, M., Weimar, J., Schrön, M., Baatz, R., and Schmidt, U.: Soil Moisture and Air Humidity Dependence of the Above-Ground Cosmic-Ray Neutron Intensity, Frontiers in Water, Volume 2 - 2020, https://doi.org/10.3389/frwa.2020.544847, 2021.

Lachenmeier, E., Mahmood, R., Phillips, C., Nair, U., Rappin, E., Pielke, R. A., Brown, W., Oncley, S., Wurman, J., Kosiba, K., Kaulfus, A., Santanello, J., Kim, E., Lawston-Parker, P., Hayes, M., and Franz, T. E.: Irrigated Agriculture Significantly Modifies Seasonal Boundary Layer Atmosphere and Lower-Tropospheric Convective Environment, Journal of Applied Meteorology and Climatology, 63, 245–262, https://doi.org/10.1175/JAMC-D-23-0020.1, 2024.

LBGR: Landesamt Für Bergbau, Geologie Und Rohstoffe Brandenburg, Bodenübersichtskarte Des Landes Brandenburg Im Maßstab 1:300,000, 2025.

Levi, M. R. and Bestelmeyer, B. T.: Digital Soil Mapping for Fire Prediction and Management in Rangelands, Fire Ecology, 14, 11, https://doi.org/10.1186/s42408-018-0018-4, 2018.

McJannet, D., Rasche, D., Marano, J., Hawdon, A., Stenson, M., and Schrön, M.: Over-Water Low-Energy Neutron Observations for Intensity Corrections Across Cosmic-Ray Soil Moisture Sensor Networks, Water Resources Research, 61, e2024WR039 727, https://doi.org/10.1029/2024WR039727, 2025.

McJannet, D. L. and Desilets, D.: Incoming Neutron Flux Corrections for Cosmic-Ray Soil and Snow Sensors Using the Global Neutron Monitor Network, Water Resources Research, 59, e2022WR033 889, https://doi.org/10.1029/2022WR033889, 2023.

Mengen, D., Jagdhuber, T., Balenzano, A., Mattia, F., Vereecken, H., and Montzka, C.: High Spatial and Temporal Soil Moisture Retrieval in Agricultural Areas Using Multi-Orbit and Vegetation Adapted Sentinel-1 SAR Time Series, Remote Sensing, 15, https://doi.org/10.3390/rs15092282, 2023.

Meyer, R., Zhang, W., Kragh, S. J., Andreasen, M., Jensen, K. H., Fensholt, R., Stisen, S., and Looms, M. C.: Exploring the combined use of SMAP and Sentinel-1 data for downscaling soil moisture beyond the 1 km scale, Hydrol. Earth Syst. Sci., 26, 3337–3357, https://doi.org/10.5194/hess-26-3337-2022, 2022.

Molenaar, R. E., Kleidorfer, M., Kohl, B., Teuling, A. J., and Achleitner, S.: Does Afforestation Increase Soil Water Buffering? A Demonstrator Study on Soil Moisture Variability in the Alpine Geroldsbach Catchment, Austria, Journal of Hydrology, p. 131984, https://doi.org/10.1016/j.jhydrol.2024.131984, 2024.

Moragoda, N., Kumar, M., and Cohen, S.: Representing the Role of Soil Moisture on Erosion Resistance in Sediment Models: Challenges and Opportunities, Earth-Science Reviews, 229, 104 032, https://doi.org/10.1016/j.earscirev.2022.104032, 2022.

Oswald, S. E., Angermann, L., Bogena, H., Förster, M., García-García, A., Lischeid, G., Paton, E. N., Altdorff, D., Attinger, S., Güntner, A., Hartmann, A., Franssen, H.-J. H., Hildebrandt, A., Kleinschmit, B., Orth, R., Peng, J., Ryo, M., Schrön, M., Wagner, W., and Wagener, T.: Integration is key to closing knowledge gaps concerning landscape subsurface water storage dynamics, Hydrol. Processes, 38, e15 320, https://doi.org/10.1002/hyp.15320, commentary, 2024.

Patil, A., Fersch, B., Hendricks-Franssen, H.-J., and Kunstmann, H.: Assimilation of cosmogenic neutron counts for improved soil moisture prediction in a distributed land surface model, Frontiers in Water, 3, https://doi.org/10.3389/frwa.2021.729592, 2021.

Patrignani, A., Ochsner, T. E., Montag, B., and Bellinger, S.: A Novel Lithium Foil Cosmic-Ray Neutron Detector for Measuring Field-Scale Soil Moisture, Frontiers in Water, Volume 3, https://doi.org/10.3389/frwa.2021.673185, 2021.

Pendergrass, A. G., Meehl, G. A., Pulwarty, R., Hobbins, M., Hoell, A., AghaKouchak, A., Bonfils, C. J. W., Gallant, A. J. E., Hoerling, M., Hoffmann, D., Kaatz, L., Lehner, F., Llewellyn, D., Mote, P., Neale, R. B., Overpeck, J. T., Sheffield, A., Stahl, K., Svoboda, M., Wheeler, M. C., Wood, A. W., and Woodhouse, C. A.: Flash Droughts Present a New Challenge for Subseasonal-to-Seasonal Prediction, Nature Climate Change, 10, 191–199, https://doi.org/10.1038/s41558-020-0709-0, 2020.

Peng, J., Albergel, C., Balenzano, A., Brocca, L., Cartus, O., Cosh, M. H., Crow, W. T., Dabrowska-Zielinska, K., Dadson, S., Davidson, M. W., de Rosnay, P., Dorigo, W., Gruber, A., Hagemann, S., Hirschi, M., Kerr, Y. H., Lovergine, F., Mahecha, M. D., Marzahn, P., Mattia, F., Musial, J. P., Preuschmann, S., Reichle, R. H., Satalino, G., Silgram, M., van Bodegom, P. M., Verhoest, N. E., Wagner, W., Walker, J. P., Wegmüller, U., and Loew, A.: A roadmap for high-resolution satellite soil moisture applications – confronting product characteristics with user requirements, Remote Sensing of Environment, 252, 112 162, https://doi.org/https://doi.org/10.1016/j.rse.2020.112162, 2021.

Power, D., Rico-Ramirez, M. A., Desilets, S., Desilets, D., and Rosolem, R.: Cosmic-Ray neutron Sensor PYthon tool (crspy 1.2.1): an open-source tool for the processing of cosmic-ray neutron and soil moisture data, Geoscientific Model Development, 14, 7287–7307, https://doi.org/10.5194/gmd-14-7287-2021, 2021a.

Power, D., Rico-Ramirez, M. A., Desilets, S., Desilets, D., and Rosolem, R.: Cosmic-Ray Neutron Sensor PYthon Tool (Crspy 1.2.1): An Open-Source Tool for the Processing of Cosmic-Ray Neutron and Soil Moisture Data, Geoscientific Model Development, 14, 7287–7307, https://doi.org/10.5194/gmd-14-7287-2021, 2021b.

Power, D., Schrön, M., Erxleben, F., Rosolem, R., and Zacharias, S.: Neptoon, https://doi.org/10.5281/zenodo.17209375, 2025.

Rasche, D., Köhli, M., Schrön, M., Blume, T., and Güntner, A.: Towards Disentangling Heterogeneous Soil Moisture Patterns in Cosmic-Ray Neutron Sensor Footprints, Hydrology and Earth System Sciences, 25, 6547–6566, https://doi.org/10.5194/hess-25-6547-2021, 2021.

Rasche, D., Blume, T., and Güntner, A.: Depth Extrapolation of Field-Scale Soil Moisture Time Series Derived with Cosmic-Ray Neutron Sensing (CRNS) Using the Soil Moisture Analytical Relationship (SMAR) Model, SOIL, 10, 655–677, https://doi.org/10.5194/soil-10-655-2024, 2024.

Reginatto, M.: Overview of spectral unfolding techniques and uncertainty estimation, Radiation Measurements, 45, 1323–1329, https://doi.org/https://doi.org/10.1016/j.radmeas.2010.06.016, PROCEEDINGS OF THE 11TH SYMPOSIUM ON NEUTRON AND ION DOSIMETRY, 2010.

Reynolds, W. D., Bowman, B. T., Brunke, R. R., Drury, C. F., and Tan, C. S.: Comparison of Tension Infiltrometer, Pressure Infiltrometer, and Soil Core Estimates of Saturated Hydraulic Conductivity, Soil Science Society of America Journal, 64, 478–484, https://doi.org/10.2136/sssaj2000.642478x, 2000.

Richter, R. and Schläpfer, D.: Atmospheric/topographic correction for airborne imagery, Tech. Rep. 565-02, ReSe Applications LLC, Wil, Switzerland, https://www.rese.ch/pdf/atcor4_manual.pdf, aTCOR-4 user guide, 2011.

Rivera Villarreyes, C. A., Baroni, G., and Oswald, S. E.: Integral quantification of seasonal soil moisture changes in farmland by cosmic-ray neutrons, Hydrol. Earth Syst. Sc., 15, 3843–3859, https://doi.org/10.5194/hess-15-3843-2011, 2011.

Robinson, D. A., Campbell, C. S., Hopmans, J. W., Hornbuckle, B. K., Jones, S. B., Knight, R., Ogden, F., Selker, J., and Wendroth, O.: Soil Moisture Measurement for Ecological and Hydrological Watershed-Scale Observatories: A Review, Vadose Zone Journal, 7, 358–389, https://doi.org/10.2136/vzj2007.0143, 2008.

Rosenbaum, U., Bogena, H. R., Herbst, M., Huisman, J. A., Peterson, T. J., Weuthen, A., Western, A. W., and Vereecken, H.: Seasonal and Event Dynamics of Spatial Soil Moisture Patterns at the Small Catchment Scale, Water Resources Research, 48, https://doi.org/10.1029/2011WR011518, 2012.

Rosolem, R., Shuttleworth, W. J., Zreda, M., Franz, T. E., Zeng, X., and Kurc, S. A.: The effect of atmospheric water vapor on neutron count in the cosmic-ray soil moisture observing system, Journal of Hydrometeorology, 14, 1659–1671, https://doi.org/10.1175/JHM-D-12-0120.1, 2013.

Scandellari, F., Attou, T., Barbeta, A., Bernhard, F., D'Amato, C., Dimitrova-Petrova, K., Donaldson, A., Durodola, O., Ferraris, S., Florian-cic, M. G., Fontenla-Razzetto, G., Gerchow, M., Han, Q., Khalil, I., Kirchner, J. W., Kühnhammer, K., Liu, Q., Llorens, P., Magh, R.-K., Marshall, J., Meusburger, K., Oliveira, A. M., Muñoz-Villers, L., Pires, S. S., Todini-Zicavo, D., van Meerveld, I., Voigt, C., Wirsig, L., Beyer, M., Geris, J., Hopp, L., Penna, D., and Sprenger, M.: Using stable isotopes to inform water resource management in forested and agricultural ecosystems, Journal of environmental management, 365, 121 381, https://doi.org/10.1016/j.jenvman.2024.121381, 2024.

Schattan, P., Baroni, G., Oswald, S. E., Schöber, J., Fey, C., Kormann, C., Huttenlau, M., and Achleitner, S.: Continuous Monitoring of Snowpack Dynamics in Alpine Terrain by Aboveground Neutron Sensing, Water Resources Research, 53, 3615–3634, https://doi.org/10.1002/2016WR020234, 2017.

Schattan, P., Schwaizer, G., Schöber, J., and Achleitner, S.: The complementary value of cosmic-ray neutron sensing and snow covered area products for snow hydrological modelling, Remote Sens. Environ., 239, https://doi.org/10.1016/j.rse.2019.111603, 2020.

Scheffler, D., Hollstein, A., Diedrich, H., Segl, K., and Hostert, P.: AROSICS: An Automated and Robust Open-Source Image Co-Registration Software for Multi-Sensor Satellite Data, Remote Sensing, 9, https://doi.org/10.3390/rs9070676, 2017.

Scheiffele, L. M., Baroni, G., Franz, T. E., Jakobi, J., and Oswald, S. E.: A profile shape correction to reduce the vertical sensitivity of cosmic-ray neutron sensing of soil moisture, Vadose Zone J., 19, e20 083, https://doi.org/10.1002/vzj2.20083, 2020.

Scheiffele, L. M., Munz, M., Francke, T., Baroni, G., and Oswald, S. E.: Enhancing Hectare-Scale Groundwater Recharge Estimation by Integrating Data From Cosmic-Ray Neutron Sensing Into Soil Hydrological Modeling, Water Resources Research, 61, e2024WR037 641, https://doi.org/10.1029/2024WR037641, 2025.

Schenk, H. J. and Jackson, R. B.: Rooting Depths, Lateral Root Spreads and below-Ground/above-Ground Allometries of Plants in Water-Limited Ecosystems, Journal of Ecology, 90, 480–494, https://doi.org/10.1046/j.1365-2745.2002.00682.x, 2002.

Schmidt, T., Schrön, M., Li, Z., Francke, T., Zacharias, S., Hildebrandt, A., and Peng, J.: Comprehensive quality assessment of satellite- and model-based soil moisture products against the COSMOS network in Germany, Remote Sens. Environ., 301, 113 930, https://doi.org/10.1016/j.rse.2023.113930, 2024.

Schrön, M., Köhli, M., Scheiffele, L., Iwema, J., Bogena, H. R., Lv, L., Martini, E., Baroni, G., Rosolem, R., Weimar, J., Mai, J., Cuntz, M., Rebmann, C., Oswald, S. E., Dietrich, P., Schmidt, U., and Zacharias, S.: Improving Calibration and Validation of Cosmic-Ray Neutron Sensors in the Light of Spatial Sensitivity, Hydrology and Earth System Sciences, 21, 5009–5030, https://doi.org/10.5194/hess-21-5009-2017, 2017.

Schrön, M., Rosolem, R., Köhli, M., Piussi, L., Schröter, I., Iwema, J., Kögler, S., Oswald, S. E., Wollschläger, U., Samaniego, L., Dietrich, P., and Zacharias, S.: Cosmic-ray Neutron Rover Surveys of Field Soil Moisture and the Influence of Roads, Water Resour. Res., 54, 6441–6459, https://doi.org/10.1029/2017wr021719, 2018.

Schrön, M., Köhli, M., and Zacharias, S.: Signal Contribution of Distant Areas to Cosmic-Ray Neutron Sensors – Implications for Footprint and Sensitivity, Hydrology and Earth System Sciences, 27, 723–738, https://doi.org/10.5194/hess-27-723-2023, 2023.

Schrön, M., Rasche, D., Weimar, J., Köhli, M., Herbst, K., Boehrer, B., Hertle, L., Kögler, S., and Zacharias, S.: Buoy-Based Detection of Low-Energy Cosmic-Ray Neutrons to Monitor the Influence of Atmospheric, Geomagnetic, and Heliospheric Effects, Earth and Space Science, 11, e2023EA003 483, https://doi.org/10.1029/2023EA003483, 2024.

Schrön, M.: CORNish PASDy—cosmic-ray neutron flavored PASDy—processing and analysis of sensor data in python, version 0.2, https://git.ufz.de/CRNS/cornish_pasdy, 2025.

Shuttleworth, W. J., Rosolem, R., Zreda, M., and Franz, T.: The COsmic-ray Soil Moisture Interaction Code (COSMIC) for Use in Data Assimilation, Hydrology and Earth System Sciences, 17, 3205–3217, https://doi.org/10.5194/hess-17-3205-2013, 2013.

Sprenger, M., Stumpp, C., Weiler, M., Aeschbach, W., Allen, S. T., Benettin, P., Dubbert, M., Hartmann, A., Hrachowitz, M., Kirchner, J. W., McDonnell, J. J., Orlowski, N., Penna, D., Pfahl, S., Rinderer, M., Rodriguez, N., Schmidt, M., and Werner, C.: The demographics of water: A review of water ages in the critical zone, Reviews of Geophysics, 57, 800–834, https://doi.org/10.1029/2018RG000633, 2019.

Srivastava, P. K.: Satellite Soil Moisture: Review of Theory and Applications in Water Resources, Water Resources Management, 31, 3161–3176, https://doi.org/10.1007/s11269-017-1722-6, 2017.

Stevanato, L., Baroni, G., Oswald, S. E., Lunardon, M., Mares, V., Marinello, F., Moretto, S., Polo, M., Sartori, P., Schattan, P., and Ruehm, W.: An Alternative Incoming Correction for Cosmic-Ray Neutron Sensing Observations Using Local Muon Measurement, Geophys. Res. Lett., 49, e2021GL095 383, https://doi.org/10.1029/2021GL095383, 2022.

Strebel, S., Bogena, H., Vereecken, H., Andreasen, M., Aranda, S., and Hendricks Franssen, H.-J.: Evapotranspiration prediction for European forest sites does not improve with assimilation of in-situ soil water content data, Hydrol. Earth Syst. Sci., 28, 1001–1026, https://doi.org/10.5194/hess-28-1001-2024, 2024.

Stumpp, C., Brüggemann, N., and Wingate, L.: Stable Isotope Approaches in Vadose Zone Research, Vadose Zone Journal, 17, 180 096, https://doi.org/10.2136/vzj2018.05.0096, 2018.

Szilagyi, J. and Franz, T. E.: Anthropogenic Hydrometeorological Changes at a Regional Scale: Observed Irrigation–Precipitation Feedback (1979–2015) in Nebraska, USA, Sustainable Water Resources Management, 6, 1, https://doi.org/10.1007/s40899-020-00368-w, 2020.

Vereecken, H., Huisman, J. A., Bogena, H., Vanderborght, J., Vrugt, J. A., and Hopmans, J. W.: On the Value of Soil Moisture Measurements in Vadose Zone Hydrology: A Review, Water Resources Research, 44, W00D06, https://doi.org/10.1029/2008WR006829, 2008.

Wang, S., Hrachowitz, M., Schoups, G., and Stumpp, C.: Stable Water Isotopes and Tritium Tracers Tell the Same Tale: No Evidence for Underestimation of Catchment Transit Times Inferred by Stable Isotopes in StorAge Selection (SAS)-Function Models, Hydrology and Earth System Sciences, 27, 3083–3114, https://doi.org/10.5194/hess-27-3083-2023, 2023.

Wassenaar, L., Hendry, M., Chostner, V., and Lis, G.: High Resolution Pore Water δ2H and δ18O Measurements by $\mathrm{H_2O_{(liquid)}} - \mathrm{H_2O_{(vapor)}}$ Equilibration Laser Spectroscopy, Environmental Science & Technology, 42, 9262–9267, https://doi.org/10.1021/es802065s, 2008.

Weber, T. K. D., Weihermüller, L., Nemes, A., Bechtold, M., Degré, A., Diamantopoulos, E., Fatichi, S., Filipović, V., Gupta, S., Hohenbrink, T. L., Hirmas, D. R., Jackisch, C., de Jong van Lier, Q., Koestel, J., Lehmann, P., Marthews, T. R., Minasny, B., Pagel, H., van der Ploeg, M., Shojaeezadeh, S. A., Svane, S. F., Szabó, B., Vereecken, H., Verhoef, A., Young, M., Zeng, Y., Zhang, Y., and Bonetti, S.: Hydropedotransfer functions: a roadmap for future development, Hydrol. Earth Syst. Sc., 28, 3391–3433, https://doi.org/10.5194/hess-28-3391-2024, 2024.

Wiegel, B. and Alevra, A.: NEMUS—the PTB Neutron Multisphere Spectrometer: Bonner spheres and more, Nuclear Instruments and Methods in Physics Research Section A: Accelerators, Spectrometers, Detectors and Associated Equipment, 476, 36–41, https://doi.org/https://doi.org/10.1016/S0168-9002(01)01385-7, int. Workshop on Neutron Field Spectrometry in Science, Technolog y and Radiation Protection, 2002.

Zhao, Y., Ling, D.-s., Wang, Y.-l., Huang, B., and Wang, H.-l.: Study on a calibration equation for soil water content in field tests using time domain reflectometry, Journal of Zhejiang University-Science A, 17, 240–252, https://doi.org/10.1631/jzus.A1500065, WOS:000372318500006, 2016.

Zreda, M., Desilets, D., Ferré, T. P. A., and Scott, R. L.: Measuring Soil Moisture Content Non-Invasively at Intermediate Spatial Scale Using Cosmic-Ray Neutrons, Geophysical Research Letters, 35, https://doi.org/10.1029/2008GL035655, 2008.

Zreda, M., Shuttleworth, W. J., Zeng, X., Zweck, C., Desilets, D., Franz, T., and Rosolem, R.: COSMOS: The COsmic-ray Soil Moisture Observing System, Hydrol. Earth Syst. Sci., 16, 4079–4099, https://doi.org/10.5194/hess-16-4079-2012, 2012.